Institut
de Ciències
Fotòniques

Neuron Guidance and Nano-Neurosurgery Using Optical Tools

Manoj V. Mathew

Barcelona, June, 2009

Universitat Politècnica de Catalunya

ICFO - Institut de Ciències Fotòniques

Chapter 6

Multimodal Optical Workstation

6.1 Overview

The work until now had shown the potential use of light to signal the growth cones of primary neuronal cells in cultures *in-vitro*. Now two important tasks were at hand. Firstly to discover the reasons behind this effect and secondly to achieve such effects *in-vivo* in a modal organism like *C.elegans*. In addition it was also aimed to achieve other neuro-manipulation effects like for example nano-surgery of axons i.e. to induce precise incisions with submicrometer accuracy *in-vivo* and study the induced effects. However we faced a major technical hurdle. Our optical system (nonlinear microscope) could at a time be used either to induce an effect (stimulation/manipulation) or to produce laser scanning images, but not both at the same time. This ability was important if we were to proceed towards achieving each of the two goals. For example if we were induce nano-neurosurgery in *C.elegans* it is important to be able to see the fluorescently tagged neurons using confocal microscopy or epi-fluorescence microscopy while the femtosecond laser beam is set to induce the surgical process. Hence we embarked on building the multimodal optical workstation, in which a multiphoton microscope with the ability to perform Two Photon Excited Fluorescence (TPEF) microscopy, Second Harmonic Generation (SHG) microscopy and Femtosecond Laser Induced Nanosurgery was build around a commercial confocal microscope where both the subsystems (confocal and multiphoton) could work independently and simultaneously.

6.2 Introduction

Ever since its introduction, the confocal microscope [14; 26; 27; 183] has emerged as a very powerful and indispensable tool for biological imaging. Its ability to provide excellent axial resolution, collect 3D images of thick fluorescently labeled specimens, together with the user friendliness and versatility of modern day commercial confocal microscopes, has made it the biologists preferred imaging tool.

Linear fluorescence microscopy, which forms the basis of confocal fluorescence microscopy, however, suffers from fundamental penalties (such as enhanced photodamage and low depth of penetration among many others) owing to the use of shorter wavelengths for excitation. Nonlinear/Multiphoton microscopy techniques like, Two Photon

Excited Fluorescence (TPEF) microscopy [45] aim to overcome these problems partly by the use of Near Infra Red (NIR) light for excitation. Harmonic Generation microscopy [Second Harmonic Generation [49] (SHG) and Third Harmonic Generation [60; 61](THG) microscopy], goes a step further by providing intrinsic contrast (without need for labeling and thus not causing photobleaching) and structural information below the resolution limit of light [184]. Moreover, a nonlinear microscope can be used to perform nanomanipulation techniques like nanosurgery [185; 186]. Hence, nonlinear microscopes provide immense possibilities in biological investigation.

A tool that would allow full use of the advantages of both a multiphoton and a commercial confocal microscope, in such a way that both systems could work simultaneously, is, however, lacking. Such a tool would allow the gathering of information using different techniques about biological active processes simultaneously. In biology, such gathering information about a biological process, using numerous techniques, in a given instant of time is of fundamental importance. For instance, during the course of an optical manipulation technique, such as nano-neurosurgery, it is particularly important to image the procedure in real time using multiple imaging techniques (e.g. brightfield and multichannel confocal microscopy). This would provide a wealth of information not only about the process itself but also about the evolution of the induced effect by this procedure. This, however, requires a device that has two independent optical systems that direct two sets of laser beams simultaneously and independently (one to induce an effect and the other to perform optical imaging). A tool with simultaneous capabilities of a commercial confocal microscope and multiphoton microscope would be, therefore, a great asset in such cases where simultaneous imaging and manipulation is required. Another interesting possibility of such a system is multimodal imaging combining linear and nonlinear techniques. This could be interesting, for instance, in cases where a particular structure could be imaged with SHG and structures around it, labeled with multicolored fluorophores, could be simultaneously imaged with multispectral confocal fluorescence microscopy.

In this work we build, for the first time to our knowledge, a nonlinear/multiphoton microscope having a commercial confocal microscope as base (inverted Nikon C1-Si) in a way that both the confocal and multiphoton sections can work independently and simultaneously. This is done without tampering with any of the confocal microscope system (like the scan and detection heads). We fully exploit all the flexibility, offered by the commercial confocal system (such as: two filter turrets, four detection ports, DIC condenser and diascopic detector) and add: 1) a separate scan head, 2) separate detection systems, both in the forward and backward directions and 3) separate control systems and software. All these features are achieved without the need to alter any of the C1-Si microscope components.

Modern day commercial confocal microscopes combine Differential Interference Contrast (DIC) microscopy, Epi-fluorescence microscopy, Multichannel Confocal microscopy, Laser Scanning Brightfield (LSBF) microscopy by diascopic detection of scanned laser beam (confocal excitation) and, recently, even Spectrally Resolved Confocal microscopy. All the above, together with fully automated components, software control and image processing /analysis tools [187] make commercial confocal microscopes very user friendly and versatile devices. The Nikon Confocal C1-Si microscope used in this work has all the aforementioned features. In addition to these features we have added the following tools:

- a) Two Photon Excited Fluorescence (TPEF) microscopy
- b) Second Harmonic Generation (SHG)/Polarization Sensitive SHG (PSSHG) Microscopy
- c) Femtosecond laser induced stimulation/manipulation.
- d) Laser Scanning Brightfield (LSBF) microscopy by detection of scanned NIR laser beam (for nonlinear excitation).

All the above mentioned features give the workstation the following capabilities:

1. Simultaneous LSBF, SHG and TPEF imaging
2. Simultaneous Confocal, LSBF and SHG imaging
3. Simultaneous Epi-fluorescence, LSBF and SHG imaging
4. Simultaneous Confocal imaging, Brightfield imaging and Femtosecond laser induced stimulation/manipulation
5. Simultaneous Epi-fluorescence imaging and Femtosecond laser induced stimulation/manipulation

The achieved capabilities 1 through 4 are being demonstrated for the first time in our knowledge. Moreover, it is the first time, in our knowledge, that all the above 5 features (1 through 5) are being offered in one single system. For each of the above mentioned capabilities, a set of illustrative results using the model organism nematode *Caenorhabditis elegans* (*C. elegans*) as the subject of study, are provided. In addition, we demonstrate one of the numerous sub features of the laser manipulation abilities; the nanosurgery in neurons of the same model organism. The combination of all the different imaging techniques with the laser manipulation asset provides us with a state-of-the-art tool for the study of real-time processes in biological functions.

6.3 The State of the art

Multiphoton microscopes are starting to be fully commercialized. The most currently existing systems are home built. Most of these systems have detection capabilities simultaneously in the forward and backward direction, enabling simultaneous SHG\THG and TPEF microscopy. Nevertheless, since these microscopes use a single scanning system, applications such as simultaneous femtosecond laser induced nanosurgery and depth resolved imaging are not feasible.

Since multiphoton and confocal microscopes share a very similar scanning and detection platform, a number of attempts have been made to convert commercial confocal systems into tools for nonlinear microscopy. This enables ease of fabrication, user friendliness and, most importantly, takes the nonlinear microscope much closer to the targeted end user: the biologists who are very familiar with the use of confocal microscopes. Most of these works [188–192] have attempted to route the ultrashort NIR light for nonlinear microscopy through the confocal scan head. This allows easy control of the microscope

by a novice user (by using the confocal microscope controls and softwares). This configuration has, however, two distinct drawbacks: 1) The confocal scan and detection heads have to be opened and modified to enable it to switch between confocal and multiphoton modes and 2) The microscope can, at a time, work either as a confocal microscope or as a nonlinear microscope, but not both simultaneously.

Commercial multiphoton microscopes that have two separate systems to direct two laser beams simultaneously (in a way that one laser is used for stimulation and the other for imaging) do exist [193; 194]. However, such systems rely on dedicated intricate optomechanical setups incorporated to the microscope and, to the best of our knowledge, they do not provide the ability to perform linear and nonlinear imaging (using the two scanning systems together) simultaneously.

There have also been attempts by research groups to set two independent laser scanning systems together to allow, for example, the ability to combine optical tweezing with multiphoton microscopy [195]. Other groups have worked on developing multimodal imaging systems in which combined multiphoton techniques, like coherent anti-Stokes Raman scattering (CARS), sum-frequency generation (SFG) imaging and two-photon-excited fluorescence (TPEF), have been demonstrated by making use of two synchronized laser scanning systems [196].

6.4 Materials and Methods

6.4.1 Construction of the microscope

The construction of the multimodal workstation is described in this section in detail and it follows the actual sequence of the workstation construction. Starting from the femtosecond laser, a) steering the laser beam onto the Galvanometric mirrors, b) describing the confocal microscope, c) steering the light inside the microscope, and d) implementation of the forward detection system. The description ends with e) a small account of the signal acquisition system, control and software used.

Steering the femtosecond light onto the galvanometric mirrors

The schematic of the setup is shown in Figure 6.1. The femtosecond laser to be used for nonlinear applications and the confocal microscope were placed in two adjacent rooms (laser laboratory and biology laboratory, respectively). A hole was drilled on the wall separating the two labs to pass the beam form the laser lab to the biolab. The main reason behind keeping the two systems in separate but adjacent rooms was to keep the microscope as close as possible to the sample preparation area to facilitate ease of transportation of the bio-samples to the microscope and at the same time keep the femtosecond laser and subsystems away from biolab conditions. The laser used was a Kerr lens mode locked Ti:Sapphire laser (Coherent MIRA 900f), which can operate both in femtosecond (160fs pulse duration, pulse repetition rate of 76MHz) and continuous wave (CW) regimes with wavelength tunable from 650nm to 900nm.

The femtosecond light beam from the laser was passed through a telescope (T1) that expanded the beam to approximately 5mm. Then the beam was passed through a Faraday Isolator (FI) to avoid any back reflections from destabilizing the laser mode lock operation. The telescope was used to reduce the beam intensity to a value below the damage threshold

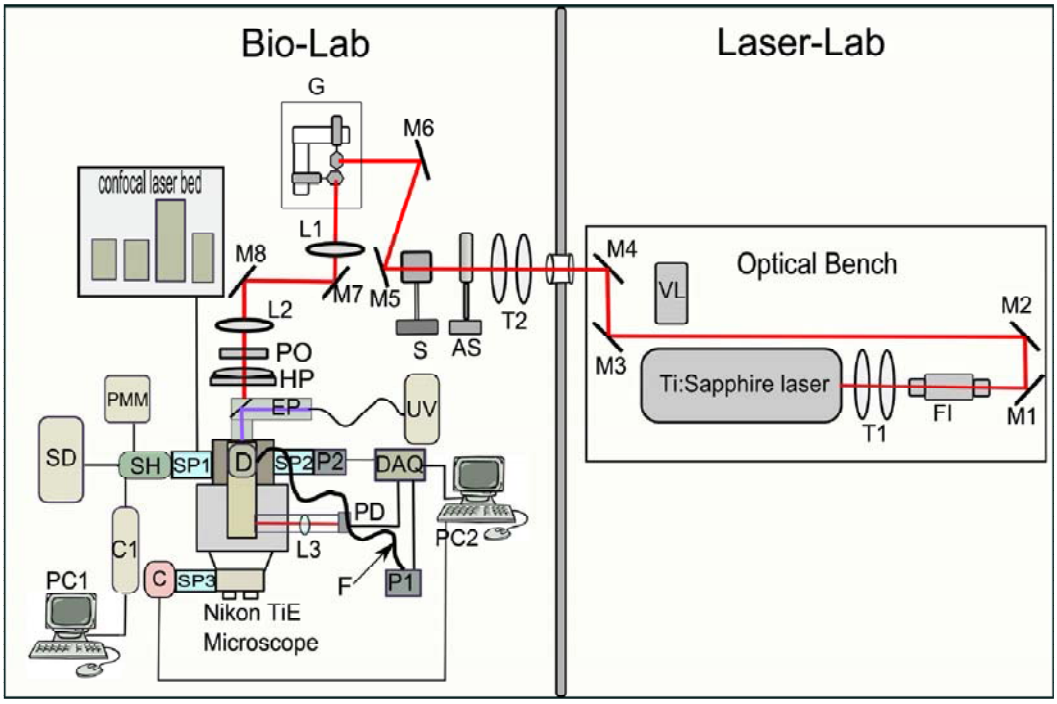

Figure 6.1: Schematic diagram of the setup developed around the Nikon C1Si confocal microscope. The setup is composed of two optical benches: one inside the laser laboratory and other in inside the biology laboratory. T-Telescope, M-Mirror, VL-Verdi Laser, FI-Faraday Isolator, AS-Attenuator set, S-Electronic Shutter, G-Galvanometric Mirror System, L-Lens, PMM-Photomultiplier Module, SD-Spectral Detector, SH-Scan Head, C1-Confocal Microscope Control box, C-CCD camera, SP-Side Port, D-Diascopic Port, F-Optical Fiber, PO-linear polarizer, HP-Half Wave plate, P-Photomultiplier Tube, EP-Epi-Fluorescence attachment, DAQ-Data Acquisition System, PD-photodiode, UV- Xenon lamp, PC-Computer and confocal laser bed with a set of four lasers (two diode lasers, one He-Ne laser and one argon ion laser).

of the FI and to compensate, to some extend, the large beam divergence caused by the significant distance between the femtosecond laser and the microscope. A set of four mirrors (M1-M4) were used to direct the beam through the wall hole in to the biolab.

Once in the biolab the beam was passed through an attenuator set (AS) containing two attenuators (attenuator 1 and attenuator 2), and an electronically controlled shutter (S). Each of the attenuators could be independently adjusted for the required power levels. The attenuators are placed side by side on a motorized translation stage (Physik Instrumente (PI), M-505) allowing one attenuator or the other to be moved in/out of the beam path under computer control. This enabled the selection of two different optical powers, under computer control, depending on which attenuator was placed in the beam path. This configuration is useful, for example, to quickly change from imaging mode to nanosurgery mode (where a lower power is used for imaging and a much higher power is used for nanosurgery). In order to reduce expense, a homemade shutter was built using a blackened metal plate mounted on an audio speaker. By applying proper voltages under computer

control the speaker membrane could be moved up/down shifting the metal plate in and out of the beam and enabling the shutter action of blocking and unblocking the laser beam. The shutter is able to switch between states in less than 100ms.

Using mirrors M5 and M6, the beam was subsequently steered onto vertical mirror of the Galvanometric System (G) (Cambridge Technology 6215H). To eliminate any losses in the 3mm galvanometric mirrors the beam was reduced to half its size (2.5mm) using a second telescope (T2) before the attenuator. The light reflected from the horizontal mirror of the Galvanometric System was passed through lenses L1 and L2 and using mirrors M7 and M8, directed into the back port of the Confocal Microscope. L1 and L2 act as a third telescope and serve two functions: 1) to image the galvanometric mirrors onto the back aperture of the objective, and 2) to expand the beam five times (to about 12.5mm) to overfill the back aperture (10mm) of the 60x high Numerical Aperture (1.4 NA) objective. L2 is a Plano convex lens of f=500mm and is kept at a distance of 500mm from the back aperture of the objective. L1 was hence chosen to be f=100mm (Plano convex) to enable a beam expansion of five times. Distance between L1 and L2 is 500+100 = 600mm and L1 was placed at a distance of 100mm from the galvanometric mirrors. These combination of lenses and distances construct the necessary imaging configuration to image the galvanometric mirrors onto the back aperture of the objective. (Details of multiphoton microscope design can be found in Reference [197]). To aid PSSHG imaging a linear polarizer (LP) and a half wave plate mounted on graduated rotating stage (HP) were placed subsequent to L2. Although the light coming out of the Ti:Sapphire is linearly polarized, there can be some degree of depolarization arising out of the numerous optics in the beam path. A linear polarizer was therefore added and rotated to provide maximum transmission. The angle of polarization of the incident femtosecond light could then be changed accurately by rotating the graduated half wave plate (HP).

The Confocal Microscope

A Nikon C1-Si (Nikon Inc, Japan) confocal laser scanning imaging system [187] built onto a Nikon inverted research microscope Ti-E is employed in the setup. The C1-Si system offers standard three channel detection as well as spectrally resolved detection modes. In addition to standard DIC microscopy, it offers LSBF imaging (by diascopic detection of forward scattered excitation laser light during confocal laser scanning) simultaneously with confocal imaging.

The diascopic detector consists of an optical fiber with one of its ends mounted inside the microscope illumination tower, between the collector lens and the lamp. The collector lens focuses the forward scattered excitation light. This light is reflected by a mirror mounted on a slider and is focused onto the fiber tip. The mirror when slided out enables the illumination light form the lamp to pass onto the collector lens to enable conventional brightfield imaging. The other end of the fiber is inserted into the C1 control box where a silicon photodiode detects the light.

The excitation for confocal microscopy is provided by a set of four lasers (two diode lasers, one He-Ne laser and one argon ion laser) mounted on a laser bed. This allows seven excitation wavelengths (405nm, 457nm, 477nm, 488nm, 514nm, 561nm and 635nm) to be used simultaneously. Light from the laser sources are combined in the laser bed and brought into the scan head (SH) using an optical fiber cable. The scan head is attached to the side port (Side Port 1) of the microscope (Figure 6.1). The emission light resulting

from confocal laser scanning is descanned by the scan head and delivered to the regular three channel detector module (PMM) or the spectral detector (SD), both of which are connected to the scan head (using optical fiber cables). The confocal microscope systems are controlled by the C1 controller along with the computer (PC1).

The Nikon Eclipse Ti-E [198] (Nikon Inc, Japan) used in the setup is a fully motorized advanced research microscope which provides DIC imaging using a DIC condenser and halogen lamp as well as Epi-fluorescence imaging using an Epi-fluorescent attachment (EP) and UV lamp. The microscope provides two Back Ports (Back Port 1 and Back Port 2)) and four Side Ports (Side Port 1 through Side Port 4) (See Figures 6.1 and 6.2 for details). The two Back Ports are positioned on top of each other. The microscope uses two motorized filter turrets where Filter Turret B is mounted on top of Filter Turret A (See Figure 6.2 for details). Excitation light transmitted in the forward direction is collected by the DIC condenser and can be directed into the optical fiber which forms part of the diascopic detector to generate the LSBF simultaneously with Confocal imaging.

Detection in the backward direction

The epi-fluorescence attachment (EP) was mounted on the first back port (Back Port 1) and the corresponding filter cubes (FC1) for epi-fluorescence microscopy are mounted in Filter Turret A. The filter turret employed standard filter sets for GFP, YFP and DsRed mounted in filter cubes FC1a, FC1b and FC1c, respectively. The femtosecond laser light was directed through the second back port (Back Port 2) into the Filter Turret B with a filter cube FC2 in which a dichroic mirror (Semrock, Inc., FF670-SDi01, T: 360nm-650 nm, R: 680nm-1080 nm) was placed. This dichroic mirror was employed to reflect the incident NIR femtosecond laser beam onto the microscope objective while allowing the fluorescent excitation light from below to pass through it onto the objective. This enables the NIR light from the femtosecond laser and the fluorescence excitation light from the confocal scan head or the epi-fluorescent attachment to coaxially pass through the objective. Similarly, this allows all generated fluorescence signals to reach the output ports for detection.

In the epi-fluorescence mode, the appropriate filter cube (FC1) in the Filter Turret A (Figure 6.2) is moved into the beam path. The excitation light form the epi-fluorescence attachment enters through the first back port (Back Port 1). This excitation light, after being filtered by the excitation filter in FC1, is reflected by the dichroic mirror in FC1 up towards filter turret B and is transmitted through the dichroic mirror in FC2 onto the objective. In confocal mode the filter sets FC1 (in Filter Turret A) are moved out of the light path (the confocal microscope does not use the filter sets inside the base microscope. The filtering is done externally) and the fluorescence excitation from the confocal scan head passes through Filter Turret A without any obstruction. It then transmits through the dichroic mirror in FC2 (in Filter Turret B) towards the objective. Here again, the fluorescence excitation light form the confocal scan head and the NIR light from the femtosecond laser can pass coaxially through the objective interacting simultaneously with the sample.

The fluorescence emission light from the sample similarly passes thorough the dichroic mirror in FC2 (in Filter Turret B). In epi-fluorescence mode this light, after passing through the barrier filter in FC1 (in Filter Turret A), passes on to a CCD camera (Hamamatsu ORKA R2) attached to Side Port 3. In confocal mode (where no filter cube is

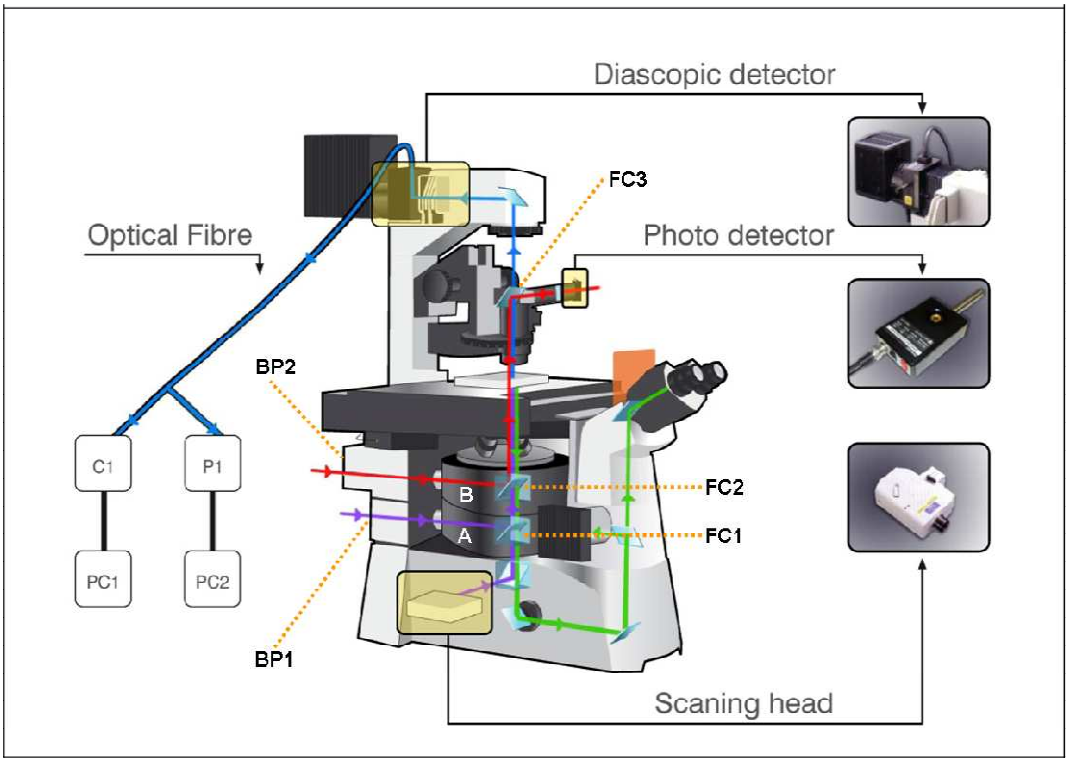

Figure 6.2: An artists impression of the multimodal microscope system with its various light paths. Green light path-backward detected fluorescence, Violet light path-epi- Fluorescence and Confocal excitation, Blue light path-Forward propagating SHG signal, Red light path-NIR excitation, PC-computer, C1-Confocal microscope control box, P1- PMT module 1, A-Filter Turret A, B-Filter Turret B, BP-Back Port , FC- Filter cube.

used in Filter Turret A) it passes to the scan head in Side port 1. In TPEF mode again no filter cubes are used in Filter Turret A and the emitted fluorescence from the sample plane is directed to Side Port 2 where a Photomultiplier Tube Module (P2) (Hamamatsu, H9305-03) detects the Two Photon Excited Fluorescence (TPEF) signal. A wide band filter (Chroma technologies, Custom GFP filter) was inserted into the PMT module to filter in the fluorescence form Green Fluorescent Protein(GFP) labeled samples. This filter could be easily swapped for others for different fluorescent markers. The ports were changed under computer control depending on the mode of operation.

A complete illustration of the different light paths that compose this multimodal system can be found in Figure 6.2, where Violet lines indicate fluorescence excitation light in confocal and epi-fluorescence modes. Red lines indicate NIR excitation light (directed onto the sample as well as transmitted through the sample onto the photodetector) for nonlinear microscopy, LSBF and nanosurgery and Blue lines indicate forward propagating SHG signal.

Detection in the forward direction

A standard DIC condenser (0.5NA front lens) (with the DIC prism and polarizer slid out) and the diascopic detector serve as a forward detection mount to aid SHG imaging. The optical fiber from the diascopic system is inserted into a second PMT module (P1) (Hamamatsu, H9305-03), which has a removable fiber input mount and an attached narrow band pass filter (Semrock FF01-434/17). The filter is used to transmit only the forward scattered SHG signal. To ensure that all light is collected when a high numerical aperture objective lens is used for excitation, the 0.5NA front lens of the DIC condenser can be replaced with a oil immersion, high NA front lens, available as a standard attachment for the DIC condenser (1.4NA, 1.92mm working distance, Nikon).

The optical fiber cable in the diascopic detector can be readily moved back and forth between the C1 control box (in case of confocal mode of operation) and the PMT module P1 (in multiphoton mode). The diascopic detector enables generation of LSBF images of the sample in confocal mode (by detecting the forward scattered confocal excitation light) while in nonlinear microscopy mode the optical fiber in the diascopic detector enables generation of SHG images.

In order to generate brightfield images in the nonlinear mode a different filter cube (FC3) is placed over the DIC condenser, which contains a second dihcroic mirror (Semrock, Inc., FF670-SDi01) that reflects NIR and transmits in visible and UV wavelengths. FC3 is simply placed on top of the slider for the polarizer in the DIC condenser (see Figure 6.2). The polarizer and the DIC prism is slid out before placing FC3. This enables the unconverted NIR excitation light to be reflected on to a photodiode (PD) (NewFocus, IR photoreceiver 2033) mounted outside the microscope, while directing the rest of the light towards the diascopic detector fiber. A collection lens L3 is used to collect the reflected NIR light and focus onto the photo detector head. Light thus detected forms the third channel in the non-linear microscopy mode to generate LSBF simultaneously with TPEF and SHG in channels 1 and 2, respectively. The nonlinear mode, hence, provides the capability for simultaneous three channel detection (TPEF, SHG and LSBF).

Signal Acquisition, Control and Software

The signals from P1, P2 and PD are collected simultaneously using a Data Acquisition System (DAQ) (National Instruments, PCI-6115) which is controlled using PC2. Hence, the controls of the confocal system are controlled using PC1 and those of the nonlinear microscopy system are controlled using PC2. PC1 and PC2 communicate with each other using Ethernet LAN.

The objective axial motion in z is performed in the confocal microscope by a motorized movement controlled by the confocal software in PC1. This control can also be done manually through a dial system provided with the microscope. In order to control the z motion automatically in the nonlinear microscopy mode, a stepper motor (Physik Instrumente (PI), C-136) under the control of PC2 was attached to this manual dial. The axial motion in z of the objective in nonlinear microscopy mode is done by PC2 by moving the stepper motor and, consequently, the manual dial. This, in turn, moves the motor controlling the motion of the objective. The distance moved by the objective can be read out in micrometers form the microscope digital display. This z motion control can be used for obtaining image stacks at successive focal planes, in the nonlinear mode of operation.

A homebuilt control software (programmed in Labview 8.2, National Instruments Cor-

poration) is employed for control, image acquisition and storage of images and metadata. The program was written to emulate, to a great extent, the features provided in the commercial confocal microscope control software. This control software runs in PC2 and controls the galvanometric mirrors to scan the NIR femtosecond laser beam in a region of interest. Moreover, it simultaneously acquires image data from three channels (LSBF, SHG and TPEF) using the signals acquired by the DAQ card from P1, P2 and PD, respectively for SHG, TPEF and LSBF. Other functions of the program include: processing of acquired images; generating JPEG images and displaying the subsequently formed images in three separate windows (in the GUI); storage of these images in specified folders, etc. In addition to all this, it allows time-lapse imaging with specified time step, generation of image stacks with specified separation in the z (by movement of the stepper motor), shutter control (for blocking and unblocking the laser beam), zooming into the region of interest using a GUI, etc.

6.4.2 Microscope sample preparation

For the illustration of the workstation capabilities two different *Caenorhabditis elegans* strains (juIs76 [unc-25::gfp] II and akIs3 (nmr-1::gfp)) expressing GFP in specific neuron types are cultured and grown in large quantities using methods reported previously [199]. A number of healthy worms are mounted on a thin 2% agar pad with an anesthetic between two 40μm glass slides. The need to use two thin glass slides comes from the need to collect information both in the backward as in the forward direction from our sample using high numerical aperture oil immersion objectives/condensers. The selected anesthetic for immobilization was sodium azide - NaN3 (0.8μl at 25mM). The mounts are sealed with melted paraffin wax for stabilization. The worm mounts were only used within a period of less than one hour in order to guarantee the worm physical condition.

6.4.3 Characterization of the point spread function

In order to characterize an imaging system measured the Point Spread Function (PSF). This was measured for both confocal and two-photon imaging systems, based on Yoo et al. (2006) [200] and Bigelow et al. (2008) [201]. Sub-microscopic G200 Polymer Microspheres (i.e. 200nm) were used as point objects. A suspension of 200nm beads in distilled water was sonicated and placed between two cover glasses and then a focal series of images of single beads were recorded in exactly the same way as for a standard biological sample to obtain the radial PSF at the focal plane. In the axial direction, a z-stack in each configuration was taken. The PSFs were acquired with 60x, 1.4NA oil immersion objective, which was used to acquire all images shown in the manuscript. Using a standard parameter to estimate the size of the image of a point, the Full Width Half Maximum (FWHM) was measured from the plot in the x and z-directions.

6.5 Operational Functioning and Results

This section starts by an image quality assessment followed by presenting a detailed description of each of the five features (see introduction 6.2) of the workstation. First a description is provided on how to configure the workstation to enable a particular feature followed by an example illustrating implementation of the feature in a biological sample. Subsections 6.5.7 and 6.5.8 describe special features relating to brightfield imaging and

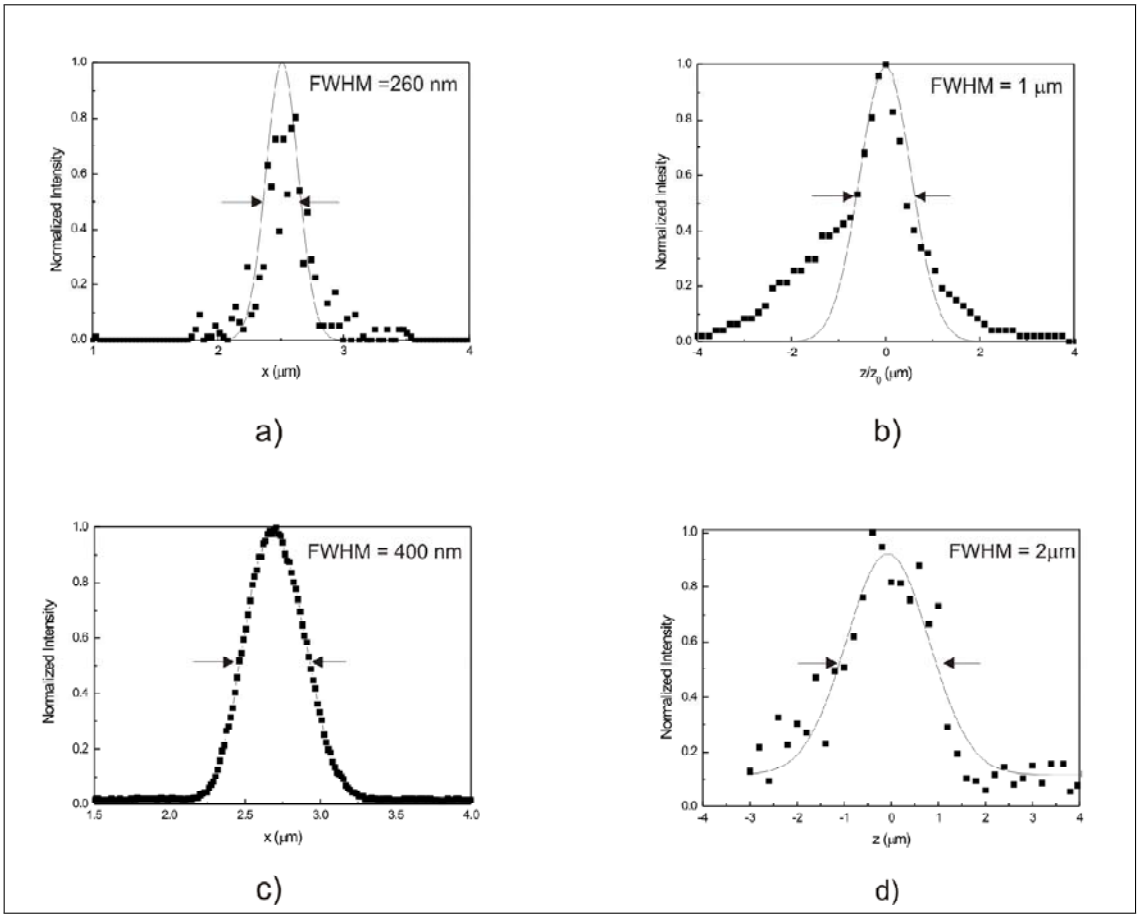

Figure 6.3: Cross-sections of the measured Point Spread Functions (PSFs) (a) along the x- and z-axis (a and b, respectively) in the confocal mode; and along the x- and z-axis in the TPF mode (c and d, respectively). The depicted curve is a Gaussian fitting to the obtained data. The diameters of the beads were 200 nm.

SHG imaging implemented in this workstation.

6.5.1 Image quality evaluation

The PSF was measured in the radial and axial directions for both Confocal and non-linear imaging modalities. The results are shown in Figure 6.3. In order to compare the performance of the different imaging systems, the Full Width Half Maximum (FWHM) was calculated from each cross section of the PSF. For the confocal imaging system, the FWHM in x-direction was around 260nm (Figure 6.3a), and in z direction was 1 micron (Figure 6.3b). The FWHM for the nonlinear configuration in the x-direction was approximately 400nm (Figure 6.3c) and in the z -direction was approximately 2 microns (Figure 6.3d).

6.5.2 Simultaneous LSBF, SHG and TPEF microscopy

In the case of Simultaneous LSBF, SHG and TPEF microscopy, none of the functions of the confocal microscope are required. The filter cube FC2 in Filter Turret B is placed

into the beam path to reflect the NIR femtosecond light (868nm) onto the objective. The control software in PC2 is used to raster scan the femtosecond laser beam in a region of interest. Emission light in the backward direction is directed into Side Port 2 to collect the TPEF signal by the PMT (P2). The filter cube FC3 is placed on top of the condenser to reflect the undepleted NIR light onto the photo-detector (PD). The optical fiber cable in the diascopic detector is pulled out form the C1 box and inserted into the PMT module (P1) to detect the SHG signal. The system acquires signals simultaneously from P1, P2 and PD thus enabling simultaneous LSBF, SHG and TPEF imaging.

The Figure 6.4 shows part of an adult *C.elegans* imaged in this modality. In this image, the LSBF image of the whole scanned region can be observed in gray scale (a), two GFP-labeled D-type motor neurons and some autofluorescence from lipofuscin granules can be observed in green color in the TPEF image (b) and the body wall muscles can be observed in red color in the SHG image (c). Images in Figures 6.4a-c were obtained simultaneously form the same scanning process. The figure also depicts a superposition of all the three image channels (d).

All the above imaging was performed using an average power of 15-18mW on the sample plane and a wavelength of 868nm. The wavelength of 868nm for excitation was chosen to suite the availability of the narrowband pass filter at 434nm for SHG imaging. This wavelength is also quite suited for exciting GFP as required for the TPEF images.

6.5.3 Simultaneous Confocal, LSBF and SHG microscopy

In simultaneous Confocal, LSBF and SHG microscopy both confocal and nonlinear microscopy subsystems work simultaneously. The filter cube FC2 in Filter Turret B is moved into the beam path to reflect the NIR femtosecond light (868nm) onto the objective and the control software in PC2 is used to raster scan the femtosecond laser beam in a region of interest. The confocal scan head delivers the excitation light through Side Port1 which also collects the fluorescence emission light from confocal laser scanning. Here excitation light from the multiphoton system and confocal system interact simultaneously with the sample. Nevertheless, the presence of the confocal pinhole, and the descanning, rejects any light coming form outside the excitation volume of the confocal system (since there is no synchronization between the two scanning systems, they do not scan the same point at any instant of time). There is, hence, no interference created in the confocal images due to the laser scanning for non-linear microscopy.

The filter cube FC3 is placed on top of the condenser to reflect the undepleted NIR light onto the photo-detector (PD) and enable LSBF imaging. The optical fiber in the diascopic detector is inserted into the PMT module (P1) detecting the SHG signal. The narrow band pass filter in the PMT module blocks out most of the noise arising out of excitation or emission light, from the confocal laser scanning. This configuration enables simultaneous confocal, SHG/PSSHG and LSBF imaging. The image acquisition in the confocal system is controlled by PC1 and that of LSBF and SHG controlled by PC2. Care has to be taken to use this configuration if the any of the wavelengths chosen for confocal excitation or the fluorescence emission lie in the same spectral region as the SHG emission.

The Figure 6.5 shows the head of an adult *C.elegans* worm imaged simultaneously using LSBF, confocal and SHG imaging modalities. The LSBF image of the whole scanned region can be observed in gray scale (a), GFP-labeled neuron (cell body and axon) can be observed in green in the confocal microscopy image (b) and the pharynx muscles can

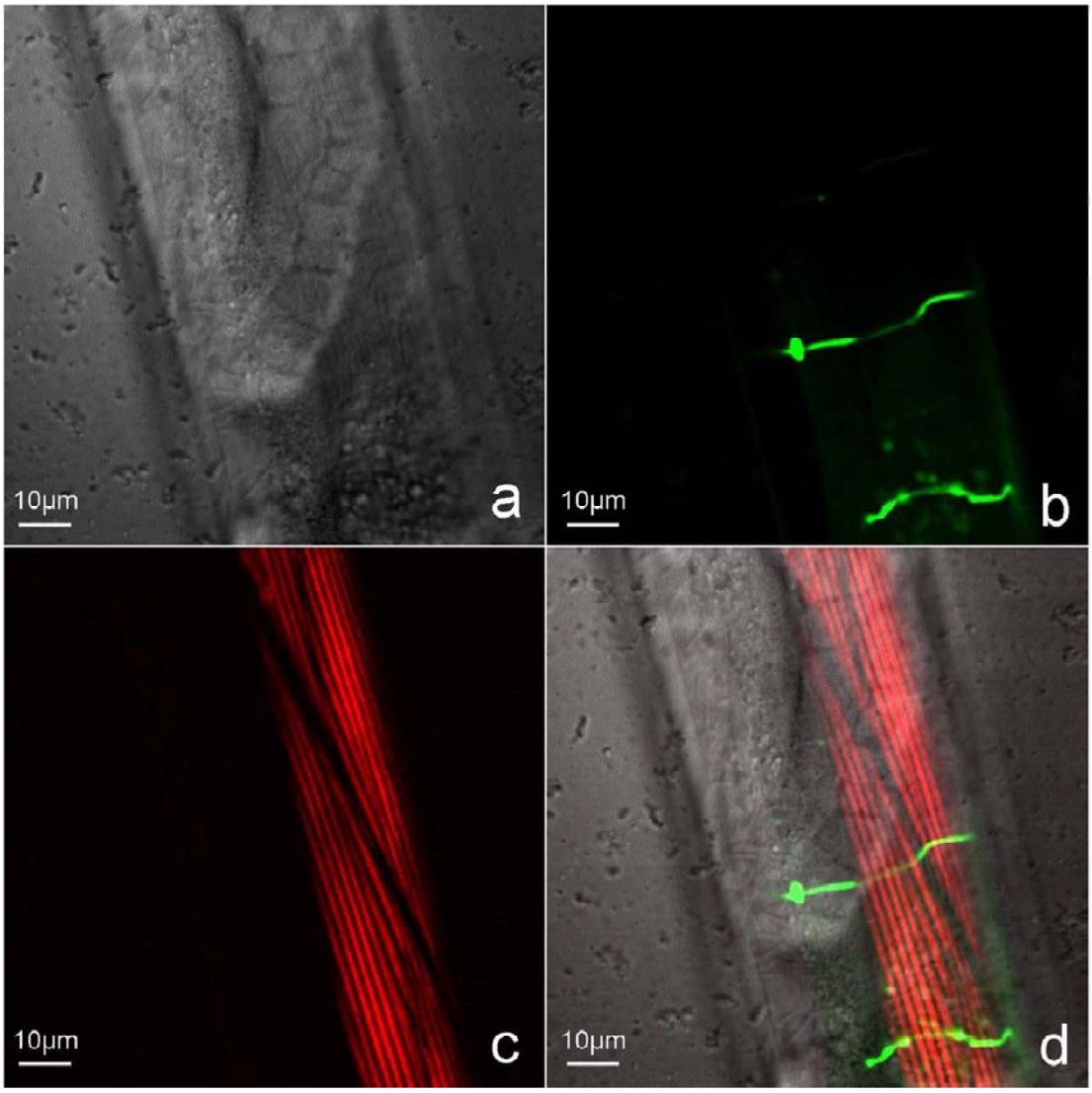

Figure 6.4: Simultaneous multimodal imaging of the midbody portion of adult *C.elegans* worm. a) Brightfield (LSBF) image of the whole laser scanned area, b) TPEF image of two D-type motor neurons expressing GFP (juIs76 [unc-25::gfp] II), c) SHG image of body wall muscles and d) superposition of all the three image channels.

be observed in cyan color in the SHG image (c). The figure also depicts a superposition of all the three image channels (d). To produce the superposition, the LSBF and SHG images are simply added since they are produced from the same scanning process. The confocal image, having used a different scanner, had to be cut and resized separately for it to be superposed onto the combined LSBF and SHG images. The green fluorescence is produced from the GFP expressed in these neurons. An excitation laser wavelength of 488nm is used to excite the GFP with the confocal system. As before, an excitation wavelength of 868nm and imaging power of 15-18mW on the sample plane are used for SHG and LSBF imaging.

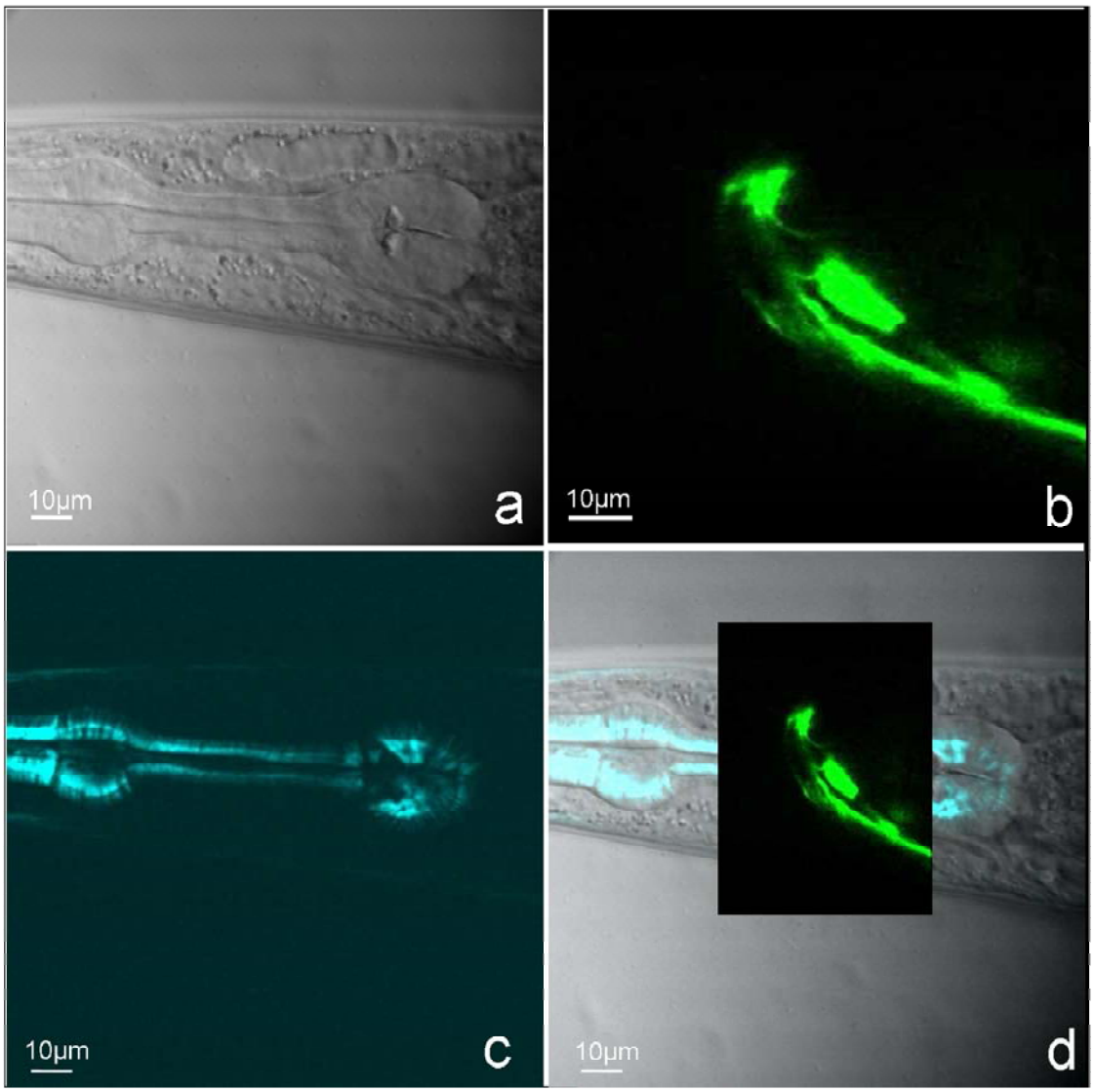

Figure 6.5: Simultaneous multimodal imaging of the head of an adult *C. elegans* worm a) Brightfield (LSBF) image of the whole laser scanned area, b) confocal microscopy image of neurons expressing nmr-1::gfp, c) SHG image of pharynx muscles and d) superposition of all the three images.

6.5.4 Simultaneous Epi-fluorescence, LSBF and SHG imaging

This mode is very similar to that presented in Section 6.5.3, except that confocal imaging is replaced by epi-fluorescence imaging. In this mode FC2 and the appropriate filter cube FC1 in the Filter Turret A is inserted into the beam path. Subsequently the epi-fluorescence attachment is switched on and Side Port 3 with the CCD camera is connected, enabling acquisition of Epi-fluorescence images by the CCD camera. Simultaneous SHG and brightfield imaging is performed as described in Section 6.5.3. The narrow band pass filter in the PMT module (P1) prevents most of the noise form the epi-fluorescence

excitation/emission from interfering with the SHG imaging. Here again care has to be taken to use this configuration if the any of the wavelengths chosen for epi-fluorescence excitation or the fluorescent emission lie in the same spectral region as the SHG emission.

Figure 6.6 shows the head of an adult *C.elegans* worm imaged simultaneously using LSBF, Epi-fluorescence imaging using the FITC filter set and SHG imaging modalities. LSBF image of the whole scanned region can be observed in gray scale (a), GFP-labeled neurons can be observed in green in the epi-fluorescence image (b) and the pharynx muscles can be observed in cyan color in the SHG image (c). The figure also depicts a superposition of all the three image channels (d). The superposition was done as in the previous section. The green fluorescence is produced from the GFP expressed in these neurons. The FITC filter cube was used for epi-fluorescence imaging. As before, an excitation wavelength of 868nm and imaging power of 15-18mW on the sample plane were used for SHG and LSBF imaging.

6.5.5 Simultaneous Confocal, LSBF and nanosurgery

A nonlinear microscope can be converted into a tool for nanosurgery. This is achieved by directing the femtosecond laser beam at very high intensity (above the damage threshold) using the scanning system to a specific point of interest. Ablation arises by the nonlinear absorption of laser light in the focal spot and can be well localized to the focal spot causing sub-micrometer incisions *in-vivo* in biological samples without, or with significantly reduced, collateral damage.

The present system provides the possibility to use two independent laser scanning systems and one of its strengths is its ability to perform real time confocal imaging while the multiphoton part is let to perform the nanosurgery or, for that matter, any other photo-stimulation/photo-manipulation.

Initially the system is made to work in multiphoton imaging mode. FC1 (in Filter Turret A) are moved out of the beam path, FC2 is inserted in and the optical fiber in the diascopic system is inserted into PMT P1. Side Port 2 is connected to enable collection of TPEF signals by PMT module P2. FC3 is inserted to enable LSBF imaging. This enables multimodal TPEF, SHG and LSBF imaging. The target selection is made using the multimodal image by defining a point in the region of interest using a GUI provided by the Labview control program in PC2. When the point is selected the program calculates the voltages to be applied to the galvanometric mirrors so that when initiated the laser beam would point to the coordinates indicated by the point in the GUI. Since each pixel in the multimodal image has a direct one to one correspondence with a galvanometric position it is straight forward to draw up a calibration that would convert the selected pixel in the multimodal image into a galvanometric position that would subsequently enable the galvanometric system to position the beam in the point indicated in the multimodal image.

Multiphoton microscopy mode is subsequently terminated and Side Port 1 is connected to initiate confocal imaging using PC1, in a region of interest (which includes the region where the surgery would be performed). The optical fiber in the diascopic system is inserted back into the C1 control box, to generate LSBF imaging simultaneously with confocal imaging. Afterwards, when the nanosurgery function in the Labview program in PC2 is initiated, it closes the shutter. Once the shutter is closed, the program removes the attenuator-1 in the attenuator set and inserts attenuator 2 (in order to let a preselected higher intensity of the laser beam pass for surgery). Subsequently the galvanometric

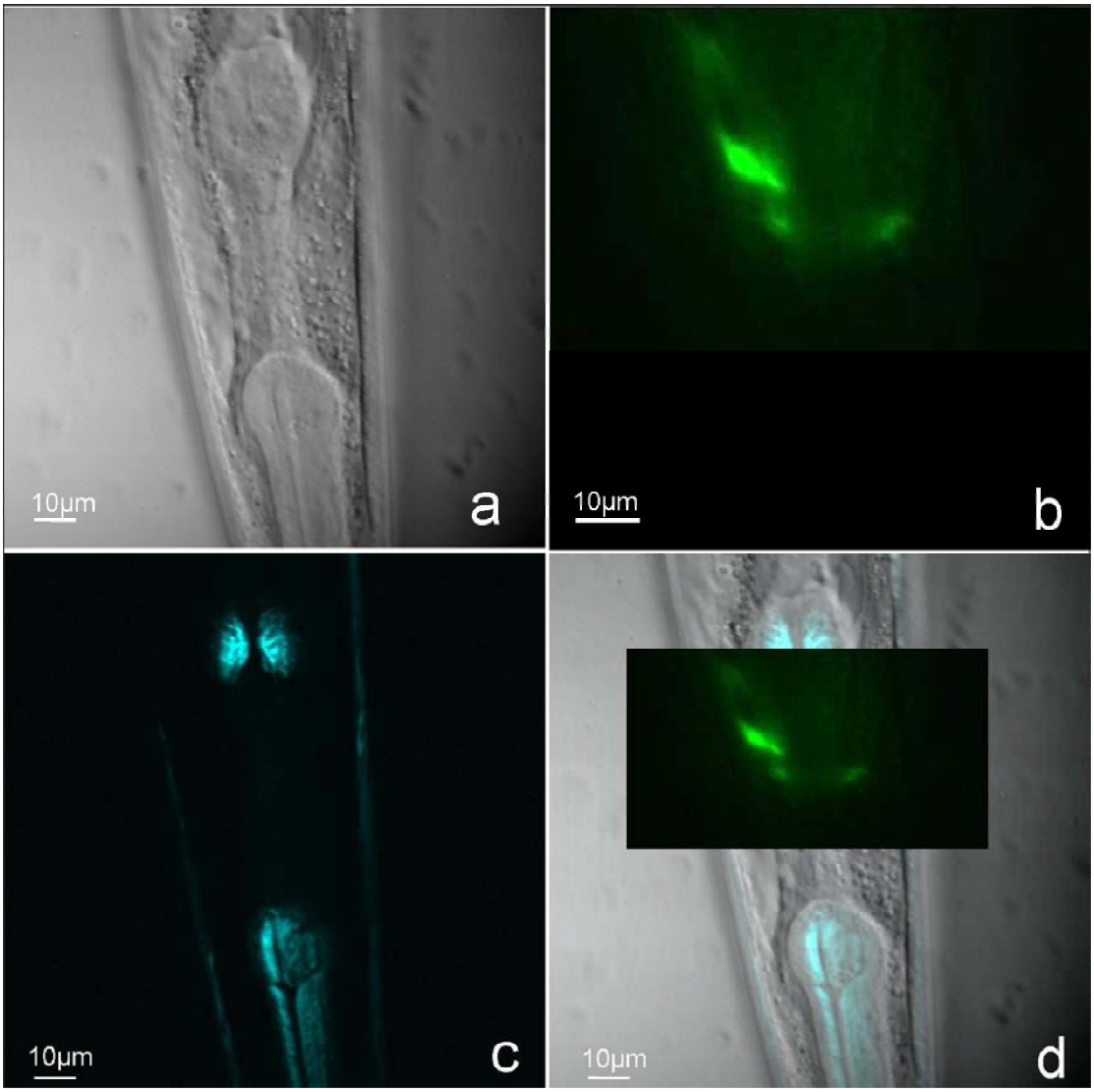

Figure 6.6: Simultaneous multimodal imaging of the head of an adult *C.elegans* worm a) Brightfield (LSBF) image of the whole laser scanned area, b) epi-fluorescence image of neurons expressing nmr-1::gfp, c) SHG image of pharynx muscles and d) superposition of all the three images.

mirrors are directed to the selected target and the shutter is opened for a specified time duration (usually few hundred milliseconds). The shutter is then closed and the attenuator 1 is placed back bringing down the optical power ready for imaging. The high laser power when let into the objective for a very short duration produces the submicrometer (usually close to diffraction limit) incision at the focal point. At the same time the confocal system generates confocal images and LSBF (using forward scattered confocal excitation light) images simultaneously. This enables high axial resolution and real time observation of the surgical process and the events taking place in the neighborhood of the surgery.

Figure 6.7 shows a time lapse image of the nanoaxotomy procedure and the subsequent

effects which were imaged using confocal microscopy. The green signal is from the GFP labeled motor neurons. The gray scale regions show the LSBF image obtained by the confocal diascopic detection system, generated simultaneously with confocal microscopy. The impact of the femtosecond laser on the axon severs it. Meanwhile a cavitation bubble is formed that produces a rupture in the cuticle. The ruptured cuticle closes back and is almost unnoticeable after a short while. This process would have gone unnoticed if the procedure of axotomy was not imaged in real time, using simultaneous confocal and brightfield imaging. The axotomy was performed using a wavelength of 880nm with an average power of about 90mW ($\sim$ 1.2nj/pulse at 76MHz repetition rate) on the sample plane, by keeping the femtosecond beam static on the axon for about 100ms using the electronic shutter. The confocal system was used to image the GFP tagged neuron using 488nm excitation along with LSBF imaging using the diascopic system of the confocal microscope.

6.5.6 Simultaneous Epi-fluorescence imaging and nanosurgery

In simultaneous Epi-fluorescence imaging and nanosurgery the configuration is very similar to the ones used in previously published works [81; 202]. Both FC2 and the appropriate filter cube FC1 (in the Filter Turret A) are moved into the beam path, the epi-fluorescence attachment (EP) is switched on and the backward fluorescence emission is directed into Side Port 3 with the CCD camera enabling acquisition of Epi-fluorescence images.

The control program selects a target using a GUI based on the CCD image. Unlike in Section 6.5.5, in this case there is no direct correspondence between galvanometric position and the pixels in CCD image. Therefore, a slightly different approach has to be adopted. A calibration procedure needs to be carried out before the experiment. A plane fluorescent sample (glass slide coated with fluorescent water color) is placed on the sample plane of the microscope prior to the experiment. The Galvanometric mirror is moved to direct the laser beam to some arbitrary point in the sample and the resulting fluorescence image is recoded by the CCD camera. The program notes the galvanometric mirrors position and the corresponding pixel position (where there is fluorescence) in the CCD image. The process is repeated a few times for different galvanometric positions. The program subsequently draws up a calibration curve based on these values relating galvanometric mirrors position to pixel position in the CCD image. The biological sample is loaded subsequently and now a target for nanosurgery can be selected merely by clicking on a point in a GUI based on the epi-fluorescence CCD image. Nanosurgery is performed as described in Section 6.5.5 using the nanosurgery function in the Labview program in PC2, while the CCD camera captures the process in real time, in the form of fluorescence images.

Figure 6.8 shows time lapse images of the nanoaxotomy procedure and the subsequent effects that take place in the vicinity of the point of surgery imaged using epi-fluorescence microscopy using the FITC filter set. The impact of the laser severs the axon and also creates a damage in the surrounding muscle.

6.5.7 Brightfield imaging

Brightfield images in this workstation can be generated in three ways: (a) by a CCD camera with bright light illumination; (b) using LSBF modality by scanning the fem-

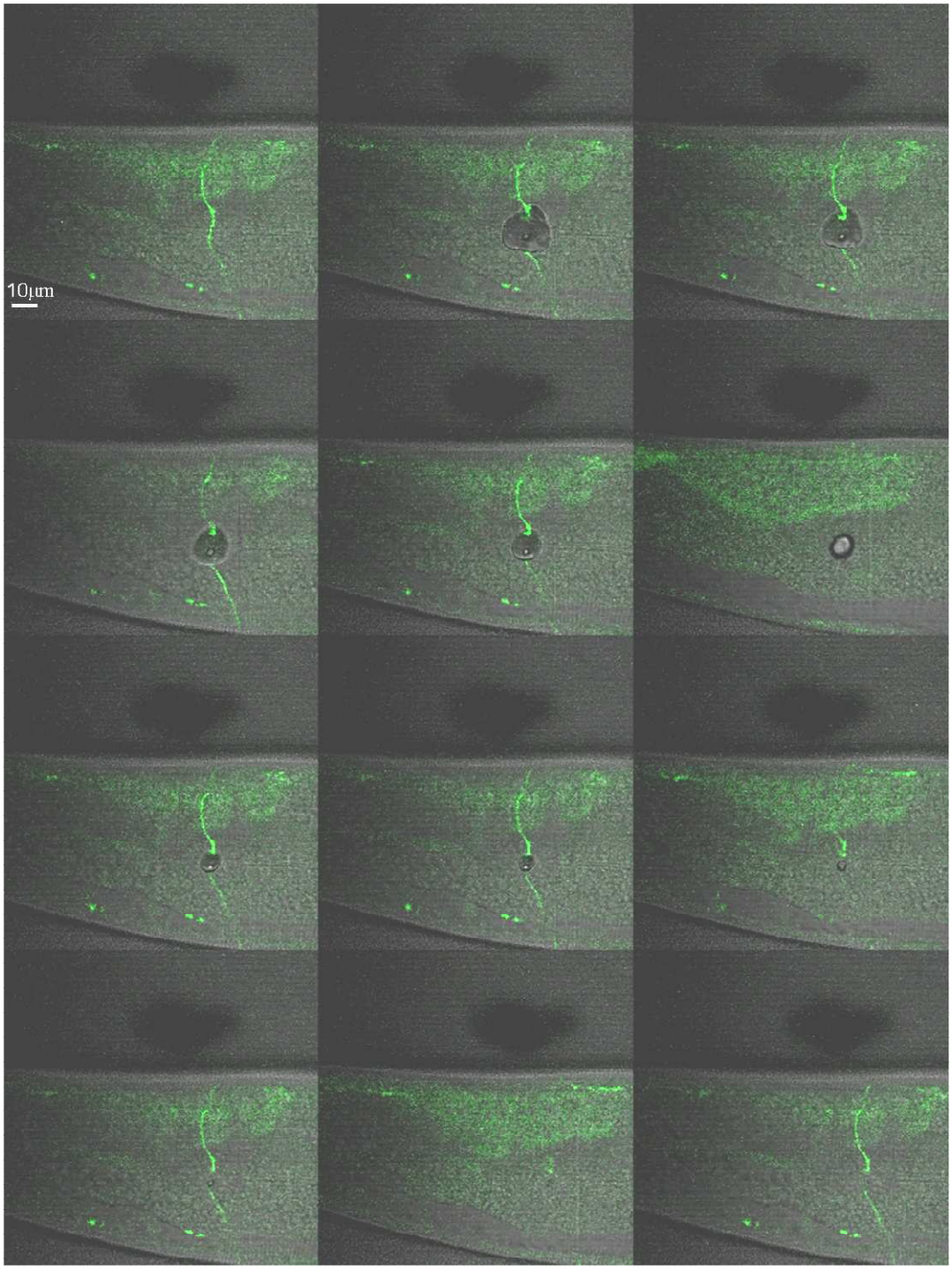

Figure 6.7: Time lapse images showing laser axotomy in an adult *C.elegans* worm imaged with both confocal microscopy and LSBF imaging.

tosecond NIR light (using forward scattered femtosecond NIR excitation light) in the multiphoton mode and c) by using LSBF in the confocal mode (detecting forward scatter

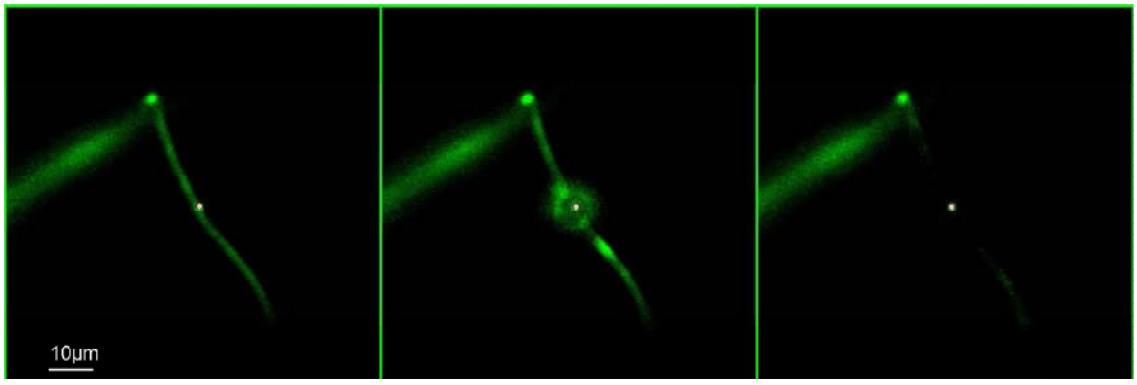

Figure 6.8: Time lapse images showing laser axotomy in an adult *C.elegans* worm imaged with epi-fluorescence microscopy.

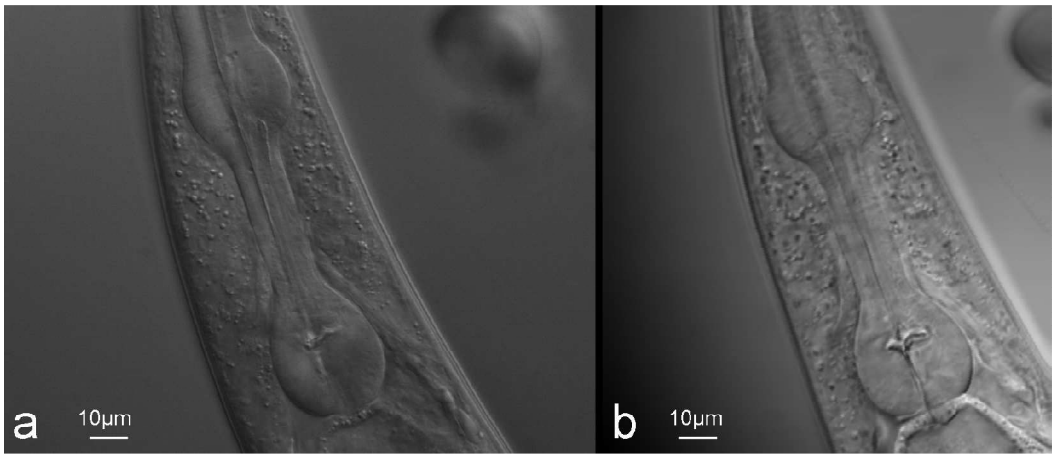

Figure 6.9: Brightfield imaging of an adult *C.elegans.* worm a) using DIC microscopy; b) LSBF microscopy.

confocal excitation light) using the diascopic detector. Figure 6.9 presents part of an adult *C. elegans* worm imaged using white light, DIC optics and CCD camera (a) compared to the LSBF image (b). The LSBF modality generates high degree of image detail, which is comparable to a great extent to the DIC microscopy image.

6.5.8 SHG and PSSHG imaging

SHG imaging, as already mentioned before, can be obtained either with a 0.5 NA or 1.4 NA condenser front lens. Ideally excitation with a high NA objective would need a high NA condenser for the collection of the emitted SHG signal. However, even with the use of the most commonly used 0.5NA condenser, that comes prefitted in most confocal microscopes, quite a high degree of image detail can be obtained. Here we present in Figure 6.10, a comparison of the SHG microscopic images of the posterior lobe of a *C.elegans* pharynx obtained using both condensers (condenser front lens with 1.4 NA (Figure 6.10a) and 0.5 NA (Figure 6.10b), respectively . It can be observed that the quality of the image obtained

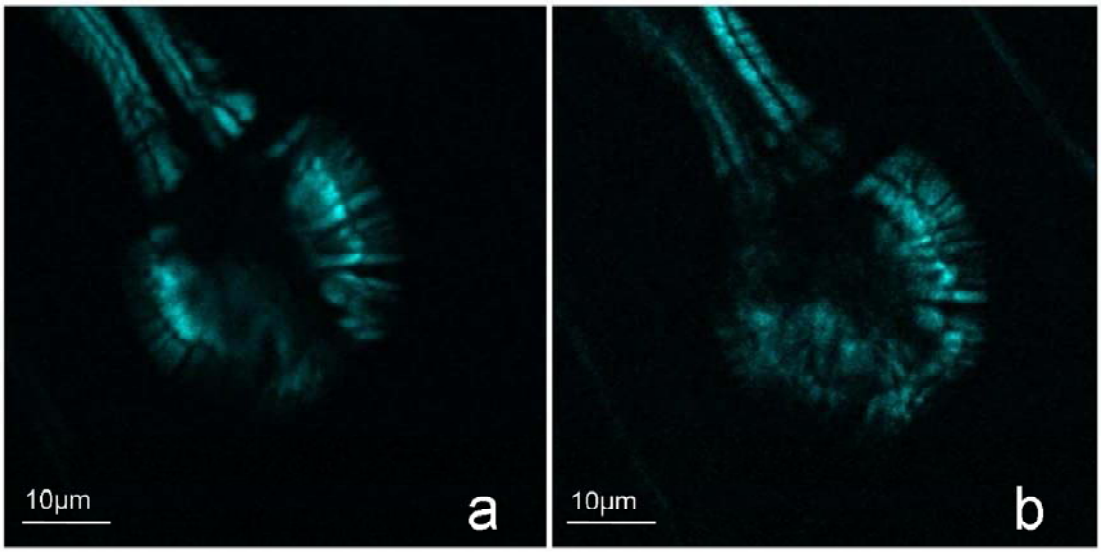

Figure 6.10: SHG imaging of *C.elegans* pharynx terminal bulb a) using 1.4NA condenser; b) 0.5NA condenser.

with 0.5 NA front lens is slightly inferior to when using 1.4NA front lens. Nevertheless, the use of the standard 0.5 NA front lens gives quite a degree of image detail.

A polarizer and a half wave plate placed outside the microscope provide an extra imaging technique: PSSHG imaging. Second Harmonic Generation microscopy can provide structural information below the resolution limit of excitation light. This is because of the coherent nature of parametric nonlinear processes and dependence of these processes on the structural organization of the interacting medium. Polarization Sensitive Second Harmonic Generation (PSSHG) imaging has been especially used for this purpose. PSSHG generation is also a capability of our multimodal workstation and can be achieved by rotating the half wave plate (HP) in fixed increments. This ability is illustrated in Figure 6.11 where PSSHG images of a starch granule (source of SHG). This modality is possible along with features in sections 6.5.2, 6.5.3 and 6.5.4. However only one isolated example has been provided for the sake of simplicity.

6.6 Multimodal imaging of *C.elegans*

Several body parts of the *C.elegans* worm were imaged using the multimodal optical workstation. Two of the examples are shown in Figure 6.12 and 6.13. Figure 6.12 shows the vulva of the nematode imaged along with the surrounding body wall muscles using a combination of LSBF and SHG imaging. Figure 6.13 shows the tail region of the nematode imaged using a combination of LSBF, SHG and TPEF imaging. Figures 6.13 a and d show LSBF images of the tail region. Figures 6.13 b , e and h show SHG images of the anal depressor muscle in the tail region. Figures 6.13 c and f show a superposition of LSBF and SHG images. Figure 6.13 g shows the TPEF image of the tail region where the autofluorescent cuticle and some autofluorescent granules can been seen. Figure 6.13i shows a superposition of the TPEF and SHG images. Figure 6.14 shows body wall muscles

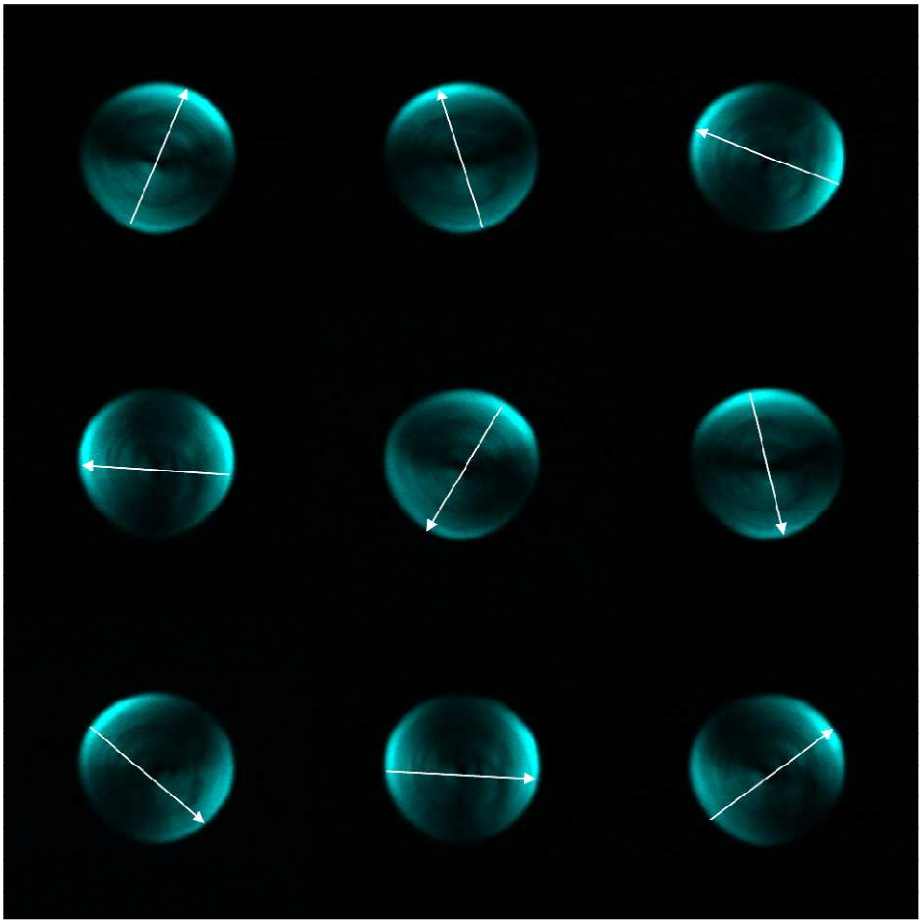

Figure 6.11: PSSHG images of a Starch granule. Images were obtained for polarization angle increments of 20^0 in counter clockwise direction.

imaged using SHG microscopy. In Figure 6.14a the individual muscle cells are visible. At a higher magnification in Figure 6.14 b the Sarcomere features (see section 4.4.2 for details) I band, H zone and M lines are clearly resolved by the multimdodal optical workstation.

6.7 Discussion

By using a commercially available confocal microscope as a base we have demonstrated how it can be adapted to form a multimodal workstation that comprises linear and multiphoton microscopic abilities. The system offers the ability for both systems to work simultaneously, hence converting the confocal microscope into a multimodal workstation. This is achieved by using off the shelf components that can be readily inserted, attached or appended externally to the confocal microscope, making the whole system very flexible to the users needs.

In this workstation we have been able to combine Confocal microscopy, Epi-fluorescence microscopy, LSBF imaging, TPEF microscopy, SHG (and PSSHG) microscopy, and nanosurgery. In addition to nanosurgery [83; 185; 186] a nonlinear microscope could be readily adapted

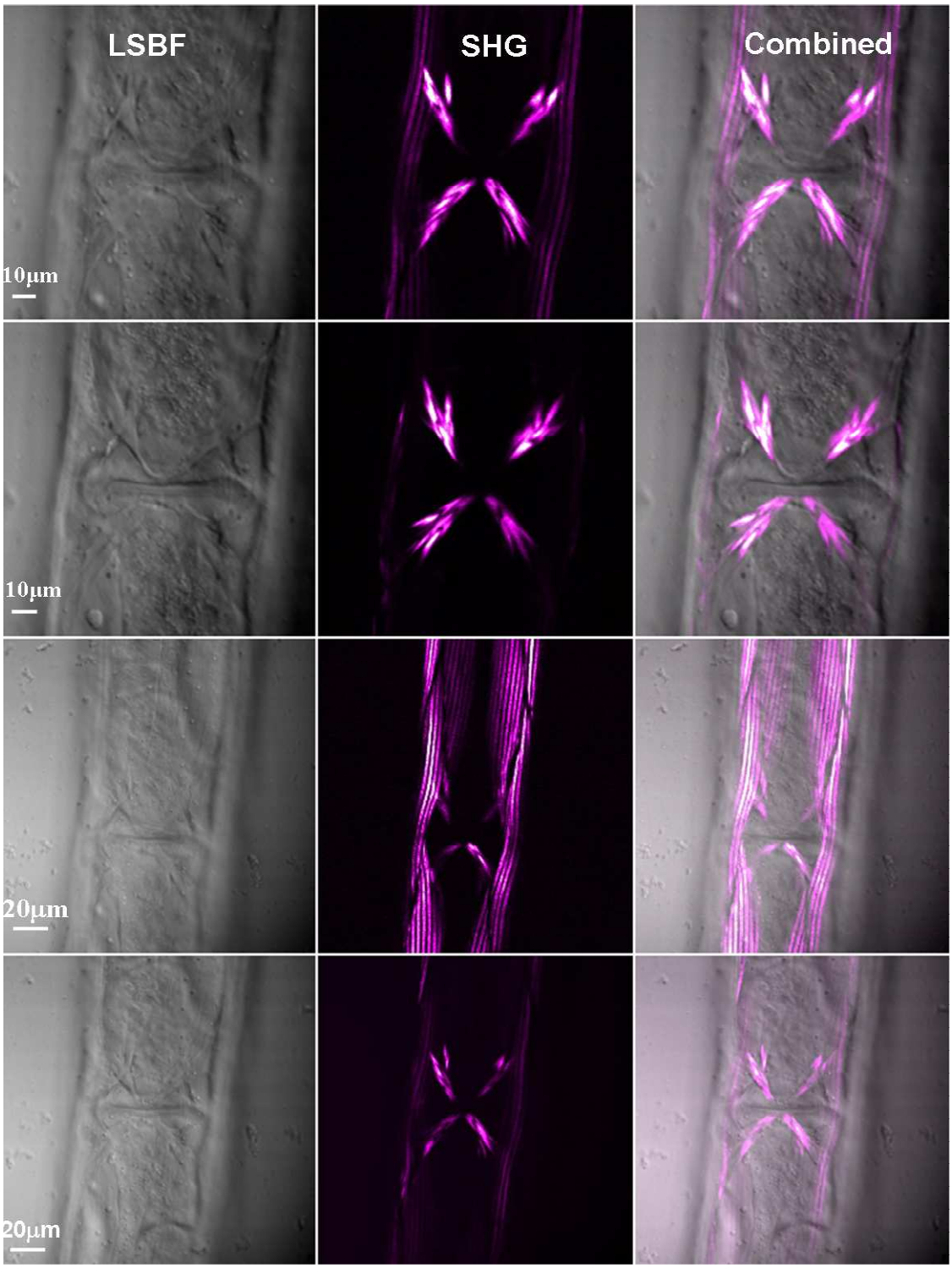

Figure 6.12: Vulva of *C.elegans*. In each row first panel shows the LSBF image, the middle panel shows the SHG image and the third panel shows the superposed LSBF+SHG image.

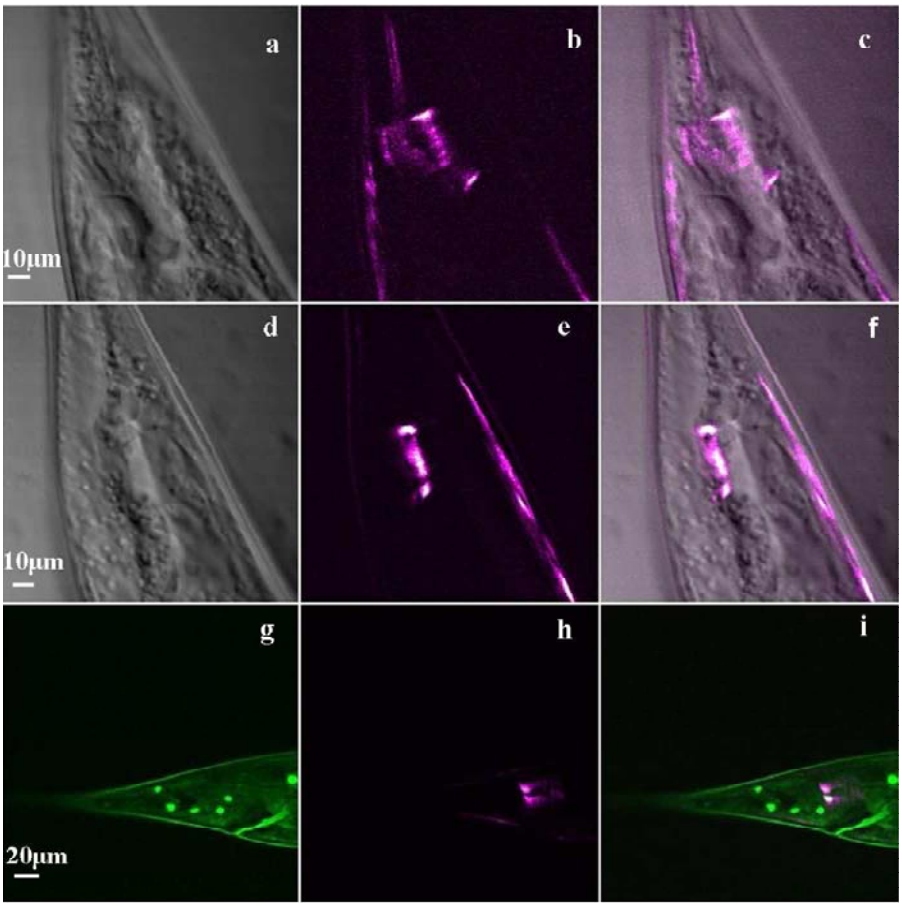

Figure 6.13: Multimodal imaging of the tail region of *C.elegans* worm. (a) and (d) LSBF images, (b),(e) and (h) SHG images of anal depressor muscle, (c) and (f) superposed LSBF and SHG images, (g) TPEF image and (i) superposed TPEF and SHG image.

as a tool for other nano-manipulation techniques, such as multiphoton stimulation [203], multiphoton uncaging of caged neurotransmitters [204], optical knock out of cell organelles [205] and intracellular chromosome dissection [77]. The setup we propose provides the possibility of combining all these techniques with real time Confocal or Epi-fluorescence imaging. The laser scanning system in the multiphoton component can also be used to induce linear effects such as optical tweezing [206; 207], photoporation [208] and Raman imaging [209], which could also be combined with simultaneous confocal or Epi-fluorescence imaging.

In general, the advantage of having two independent laser-scanning imaging sets onto one microscope is that while one set is inducing an optical effect (such as optical tweezing, nanosurgery or photostimulation) the other set can be imaging this procedure simultaneously in real time. A practical example is presented in this work where while the multiphoton set is performing nanosurgery, the confocal part is imaging this process in real time. This provides a way to reveal many events that happen along with the nanosurgery procedure. The illustrative examples for nano-neurosurgery in this paper were specially

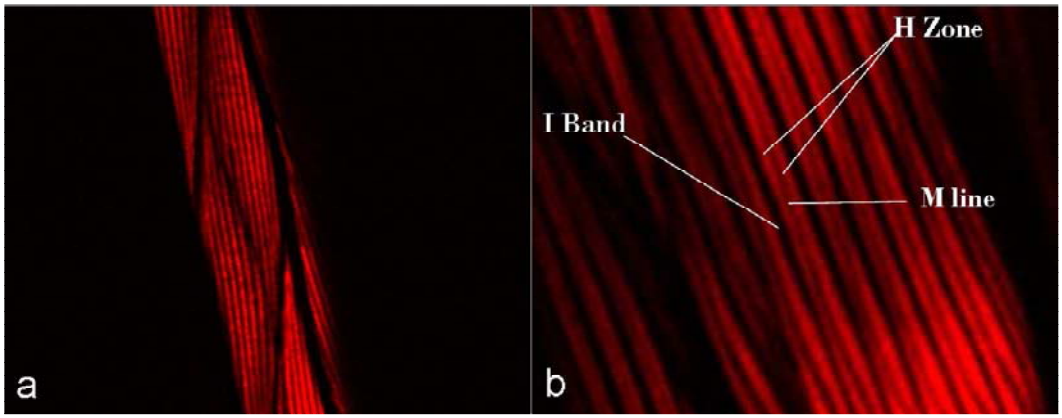

Figure 6.14: SHG images of the bodywall muscle in *C.elegans*. a) Bodywall muscle with individual muscle cells clearly visible. b) At an higher magnification the Sarcomere features I band, H zone and M lines are clearly resolved.

selected to reveal effects like muscle and cuticle damage, that sometimes happen along with the process of nanosurgery, but goes unnoticed due to the lack of simultaneous imaging functionality.

Such microscopy systems, where simultaneous imaging and optical stimulation is possible, do exist commercially [193; 194]. The presently available commercial system has both the imaging and stimulation part both based on nonlinear excitation. This is quite distinct from the work here presented where we combine linear and non-linear imaging techniques that can be used simultaneously, in addition to the multiple applications for photo manipulation/stimulation (linearly or nonlinearly). Moreover, the work here presented emphasizes our efforts for upgrading, in a cheap and natural way, a fully automated commercial confocal microscope without compromising any of its functions.

Most laboratories have confocal microscopes as a central facility and the possibility to mechanically/electronically modify the confocal microscope into a multiphoton microscope is seldom possible. This work demonstrates the possibility of a conversion without the need for any irreversible modifications. The normal functionality of the confocal microscope in this workstation is, in no way, affected. The components added directly onto the microscope are standard off the shelf attachments available from the microscope manufacturer. The rest of the components are placed external to the microscope. This allows to readily return the microscope back to its original status quo. In addition, the excitation laser beam of the nonlinear system is brought in from an adjacent room into the confocal facility. This provides a solution to a frequently encountered situation in which there is little possibility of placing systems (like femtosecond lasers) and subsystems in the same facility as the confocal microscope station. The fact that each system (both the linear and the nonlinear system) has the characteristics of a dedicated system is also a great asset of this workstation. In principle, provided that there are available ports with sufficient transmission and there is a prospect for having two filter turrets (or simply a possibility to include an extra dichroic mirror and enough space for the entrance of an external laser beam), there is a clear prospect for similar upgrades to other confocal microscopes.

Brightfield images generated by the conventional microscopy methods are usually

achieved by a CCD camera with bright light illumination. In multiphoton microscopy the capture of these images needs to be done before or after the sample is imaged/manipulated. This presents two distinct drawbacks: 1) Brightfield image cannot be generated simultaneously with multiphoton imaging and 2) there is no direct correspondence between the two image sets (Brightfield and multiphoton) in terms of pixel resolution and imaged area. Brightfield imaging using forward scattered excitation light, as presented in this work, obviates these drawbacks allowing simultaneous Bightfield imaging and multiphoton imaging. Since both the image sets (LSBF and multiphoton) are generated from the same scanning process, there is a direct one to one correspondence between the brightfield image and SHG/TPEF images and a perfect superposition of these two/three imaging modalities is obtained. This helps a great deal in precisely locating the origin of SHG/TPEF in the biological specimen. Moreover in time lapse imaging of dynamic processes it is very helpful to have a brightfield image for every corresponding TPEF/SHG image, so that these dynamic processes could be precisely mapped onto the body of the biosample.

The present C1-Si confocal system features simultaneous excitation with seven different wavelengths and detection in either three channel or spectrally resolved modes. Simultaneous excitation with multiple wavelengths for TPEF would require a number of femtosecond lasers working at different wavelengths. This is, obviously, cost and space prohibitive. Accordingly, when it comes to multi spectral excitation and detection the confocal microscope still holds an edge when compared to TPEF microscopy. The described workstation provides the user with the flexibility of combining SHG and brightfield imaging with, either confocal imaging or TPEF imaging (depending on whether advantages of TPEF or confocal imaging are required).

In order to achieve SHG microscopy, a forward collecting mount is normally required, since the harmonic generation signal preferentially travels in the forward direction. In setups used by most research groups for this purpose, forward mounts, specially fabricated for the purpose, are used. In this work the standard 0.5 NA DIC condenser, in conjunction with the diascopic detector, that come prefitted with most commercial confocal microscopes, were directly used to collect the forward scattered SHG signal without any overhead. To collect in the full numerical aperture while excitation with high NA objectives a standard 1.4 NA oil immersion DIC condenser replaces the 0.5 NA DIC condenser providing very high quality SHG images. A polarizer and a half wave plate placed outside the microscope provide an extra imaging technique: PSSHG imaging that can provide structural information below the resolution limit of excited light.

Nonlinear microscopes are increasingly being used not only for nonlinear imaging but also, after some minor changes, for cell/tissue/substrate manipulation techniques. A common drawback when performing techniques like nanosurgery is that imaging cannot be performed simultaneously with the nanosurgery. Real time imaging is essential to capture the surgery progression as well as events taking place immediately after the surgery in and around the region where surgery was performed. A number of works have used the Epi-fluorescence microscopy in conjunction with nanosurgery for real time imaging of the surgical procedure [81; 202]. Epi-fluorescence microscopy, however, does not provide the axial resolution or clarity of nonlinear microscopy or confocal microscopy. The setup described here provides real time confocal microscopy along with nanosurgery.

Even though epi-fluorescence microscopy does not provide the sharpness in image quality or the depth resolution as in confocal microscopy, it might prove useful. Epi-

fluorescence microscopy using a CCD camera is much faster than laser scanning techniques. Moreover, combining Epi-fluorescence microscopy with nanosurgery or SHG and bright-field imaging enables a number of features of this workstation when built on a standard microscope (without the confocal imaging attachment). This could be, in many situations, an economical alternative to a confocal system.

6.8 Prospects

Although the presented results in this work demonstrate only a small subset of the capabilities of the system, numerous other applications exist in which combined linear and non-linear optical techniques, or induction of an optical effect with one system while imaging with the other, are required and aimed for. All such applications could make use of this workstation. In this work we present some practical applications of the developed workstation in the field of cell biology. Nevertheless, there is a vast field of possible applications that could benefit with the use of this tool.

The presented system has great potential and large room for prospective improvements. THG can replace SHG if longer wavelengths for excitation are used. It is also possible to image THG and SHG simultaneously by adding another dichoric mirror in a fourth filter cube (FC4) that could be placed above the filter cube FC3 (positioned on top of the condenser). If a dichroic is so selected, so as to reflect the THG, it could be detected by a detector placed outside the microscope while the SHG could be allowed to propagate into the optical fiber in the diascopic detector. Since THG microscopy is sensitive to interfaces like membranes, in *C.elegans* it can be used to image hypodermis, lipid depositions in the tail and intestine, sub-cellular organelles, inclusions, cavities, cuticle in the body wall muscles, the linings of the animal pseudocoelomic cavity, pharyngeal epithelium in buccal cavity, boundaries of the pharyngeal muscles, contours of individual cells inside embryos etc: [210].

Presently the software that operate the confocal and the multi-photon systems are independent and running in different computers. In the near future the software can be brought together onto one single platform. This would provide better synchrony and coherence among the two systems, especially when it comes to defining a common region of interest, time lapse imaging, etc.

The nonlinear component of the system can also be used to induce linear effects, like optical tweezing, merely by switching the laser mode to CW. For example, while the second system performs optical tweezing, the confocal or epi-fluorescence component could be imaging the process in real time.

In summary, the multimodal workstation described here offers a highly flexible, versatile and complete solution, providing an extremely useful tool of investigation in biology simultaneously using a combination of linear and non-linear techniques. This upgrade can be incorporated in any commercial confocal microscope provided that there are available ports and there is a prospect for having two filter turrets (or possibility to include an extra dichroic mirror and enough space for the entrance of an external laser beam).

Chapter 7

Nano-Neurosurgery

7.1 Overview

The use of laser as a scalpel in both medicine and biology is starting to be widespread with several different applications. Femtosecond laser axotomy has proven to be a powerful tool for the study of subcellular phenomena especially, neuron regeneration in the earthworm *Caenorhabditis elegans*. The axotomy is an active process that lasts for a very short duration of time and that can (depending on the circumstances) lead to varying degree of collateral damage. Currently, real time imaging of the Nano-neurosurgery procedure is limited to linear fluorescence techniques. This chapter describes various choices of imaging techniques, to assist in the study of the dynamics of the process of laser Nano-neurosurgery. With this tool several dynamic phenomena concomitant with laser nanosurgery in *C. elegans* were observed and imaged. Some of these dynamic phenomena, like muscular contraction and single muscle cell stimulation, have been imaged for the first time during nano-neurosurgery of *C. elegans*. Moreover, in addition to real time imaging and damage assessment in neighboring tissues, this chapter describes an original technique to determine minute damages in close by tissues such as muscle. We propose the use of Second Harmonic Generation (SHG) microscopy as a novel tool to assess collateral damage. These studies put forward novel uses of the multimodal optical workstation setup that allows simultaneous imaging, by both linear and non-linear imaging modalities, and cell manipulation.

7.2 Introduction

7.2.1 The state of the art

Light can be used as a powerful tool for biological and medical applications. Short pulsed lasers have been used for more than 20 years in the manipulation and disruption of transparent materials, including biological materials. One of the most significant advantages of femtosecond laser ablation is its confinement primarily to the focal volume ($<$ 1 femtoliter) of the tightly focused laser beam, owing to the involvement of nonlinear mechanisms in the ablation process. Chemical alteration by ionization, mechanical and thermal effects of the shock wave and cavitation bubble can lead to severe changes in the

targeted material. Nevertheless, considering that the affected volume of the mentioned effects is on a microscopic level, these effects can be exploited for the obliteration of many intended targets. Moreover, there are ways to get control over the affected volume such as tight focusing.

Some of the applications of femtosecond lasers in living systems are: neuronal axotomy in *C.elegans* [81], development disruption in *Drosophila melanogaster* embryos [211], subcellular nanosurgery in cell cytoskeleton [212] and mitochondria [213] and generation of micro-strokes [214]. In addition, there is a commercially available laser surgery tool which is currently in use for human eye surgery [215].

The use of ultrashort near infra red wavelengths (NIR), which translates into high tissue penetration depth, and high peak power at very low pulse energy allows full control of laser ablation on a sub-micrometer level. This discloses on a whole new window for laser nanosurgery as a non invasive powerful surgery technique that can be applied in a vast range of biomedical areas.

A deep understanding of the functioning of neuronal circuits responsible for the simplest behavioral action is one of the biggest endeavors of neurobiology. Moreover, understanding the biological basis of nerve regeneration can lead to tremendous possibilities in development of new therapies for neurological diseases. The use of fully studied model organisms that exhibit a simple nervous system that can be easily studied has proved to be an influential assignment. The 302 neurons of the *Caenorhabditis elegans* (*C.elegans*) hermaphrodite nervous system and its large and complex behavioral repertoire are attractive attributes. Moreover, its organization and synaptic connections have been thoroughly studied.

Single *C. elegans* neurons were first used as targets for laser surgery by Yanik *et.al.* [81] for the study of motorneurons regeneration *in-vivo*. In this study individual D-type motorneurons were precisely cut with focused femtosecond laser pulses inside the anesthetized worm inducing a behavioral response (after surgery the worms were not able to move backwards; the shrinker phenotype). Within 24 hours most of the targeted neurons re-grew and restored their function which allowed the worms to regain their characteristic body movement. In a later work the damage threshold of femtosecond laser induced nanoaxotomy in *C. elegans* was characterized and parameters like the extent of damage, and the statistical rates of axonal recovery as a function of laser parameters were studied [216]. Femtosecond laser nanoaxotomy *in-vivo* and subsequent nerve regeneration were also demonstrated on a microchip [217]. The microchip enables immobilization of the *C. elegans* worm without the use of anesthetics leading to faster regeneration of the axotimized neurons.

Laser ablation has been extensively used in *C. elegans* embryos targeting certain cell precursors to gain knowledge of its behavioral effect in larvae/adulthood stages [218]. Nevertheless, the applied technique mainly targets cell bodies (killing the complete cell) and uses ultraviolet wavelengths (mostly around 440nm) implying higher tissue absorption and, therefore, bigger induced surrounding damage. Employing near infrared (NIR) wavelength ultrashort lasers for the laser ablation/cut has a considerate amount of advantages over the commonly used laser UV guns for cell ablation. The leading advantage is certainly the confinement of damage to a submicron volume area. Femtosecond lasers, with low repetition rates (KHz) and high repetition rates (MHz) have been successfully employed to precisely cut, within milliseconds, individual neuronal processes [219]. This

allows not only the study of the individual cell effects and function but also a much more exhaustive study at different levels of the neuron's synaptic branches and regeneration properties [202; 220–222].

7.2.2 Imaging Nano-neurosurgery dynamics

So far, real time imaging of laser manipulation techniques, such as laser axotomy in *C. elegans*, has only been done with Epi-fluorescence and DIC microscopy [202]. This can, therefore, be a drawback since many dynamics that happen along with the procedure could be missed due to the lack of simultaneous high axial resolution imaging. The multiphoton/nonlinear microscope, when used to perform nanosurgery, can also be used to obtain high axial-resolution images of the targeted area before and after the process of nanosurgery is performed. This way of imaging before and after, however, has the drawback that many dynamic phenomena that occur during the nanosurgery procedure can be missed out due to the lack of simultaneous imaging capability. A tool that provides a combination of different imaging modalities that allows imaging the process of nanosurgery and the various phenomena taking place along with it in real time is yet missing. Moreover, both during the process and immediately after the laser axotomy process occurs, a close examination of the surrounding structures needs to be preformed in order to correctly assess for the possible collateral damage.

In this study we present, the possibility to simultaneously image highly dynamic processes occurring during the laser nanosurgery of neuronal axons in *C. elegans* with high axial resolution imaging techniques. Moreover, we present the possibility of using the multimodal workstation that allows simultaneous imaging by both linear and non-linear imaging techniques while, and immediately after, the nanosurgery procedure.

High resolution (both axial and radial) real time imaging of the process is essential for a correct assessment of the efficiency of the surgical process. Likewise, real time imaging is critical for the accurate study of the process as a physical phenomenon. With the use of the multimodal workstation several active processes related with the laser axotomy were imaged in real-time. These can be used for the improving the above-mentioned laser manipulation tool and provide valuable information for the study of the interaction between laser and biological samples.

We provide, therefore, the possibility to combine imaging techniques including confocal fluorescence microscopy for simultaneous imaging of the *in-vivo* nanosurgery procedure, providing a powerful tool to study a wide range of physiological processes *in-vivo* in *C.elegans*.

7.2.3 Damage assessment

In all studies so far the assessment of the cut/damaged area was done by visual examination of the post surgical images or by physical (theoretical) determination of the affected volume considering the characteristics of the laser [81; 216]. Moreover, damage evaluation was done by simultaneous inspection (with either Brightfield or Differential Interference Contrast (DIC) imaging or by Epi-fluorescence imaging) while cutting. More detailed information can be retrieved, afterwards by imaging the targeted area by Confocal microscopy. Neuron cut effectiveness can be outlined using similar cuts done in phasmid neurons together with DiO and DiI staining and by observing certain physical characteristics of ablated tissues [81].

In this work the ability to simultaneously obtain high axial resolution confocal microscopy and brightfield images while performing axotomy provides the ability to observe the process of axotomy and the dynamics happening in the surrounding structures during this process. This in addition to providing a better insight into the the various dynamics happening during the course of nanosurgery, helps detect possible collateral damage. Moreover, we present a promising damage assessment technique to determine minute damages in nearby tissues such as muscle. We propose the use of Second Harmonic Generation (SHG) microscopy performed post-surgically as a means to detect the presence of damage if any to the muscles surrounding the axons as a result of the axotomy procedure. In addition *C.elegans* strains with muscles genetically tagged with fluorescent proteins enables the use of confocal microscopy to detect damaged surrounding muscles in real time. These abilities are provided by the multimodal optical workstation that provides simultaneous imaging, by both linear and non-linear imaging techniques, and a cell manipulation tool (see chapter 6).

7.3 Methodology

7.3.1 Worm mounting

C.elegans strains were maintained on Nematode Growth Media (NGM) agar plates using standard procedures [199]. To visualize D-type motor neurons, we used the transgenic strain juIs76 [unc-25::gfp] II, which has its D-type motor neurons fluorescently labeled. For direct visualization of possible collateral damage in closely neighboring body wall muscles we used RP1 that expresses a membrane-anchored YFP (Mb::YFP) [223] in all body wall muscles from a transgenic array called trIs10. The worm cultures were synchronized and single L4 larvae were mounted on 2% agar pads with 0.8μl of 10mM Levamisole between two 40μm glass slides. The use of two thin glass slides arises from the need to collect information in the forward direction (in contrary to the standard backward signal collection as in Confocal and Epi-fluorescence microscopy) from our sample. Glass slides were sealed with melted paraffin for sample stabilization.

7.3.2 Axotomy and simultaneous imaging

Axotomies were performed on the commissures of the worm's D-type motorneurons. Selection of the axon cut region was done on the most dorsal part of the axon just after its association with both the dorsal and ventral cord (1-2μm away from the dorsal cord) on the first one third of the axon. This allowed the presence of the body wall muscle quadrants on a different z position (but on the same xy plane). This enabled us to have the muscular tissue to be as close as possible to the region of axotomy and was intended to perfect the Nano-neurosurgery procedure. The presence of neighboring body wall muscles was confirmed by SHG imaging.

In each worm three neuron cuts were made on the level of the 3 most posterior commissures of the VD motorneurons running from the left side of the animal. The commissures' targets were selected using a graphic user interface GUI based on the combined Two Photon Excitation Fluorescent (TPEF) image of the neurons and Second Harmonic Generation (SHG) image of the muscle. This helped selecting the target on the neuronal commissure with respect to the muscle. In addition this allowed us to certify that we were

in the precise focal plane for an efficient cut. For details of the neurosurgery procedure see section 6.5.5. The axotomies were performed using a wavelength of 868nm with an average power of about 90mW (1.2 nj/pulse at 76 MHz repetition rate) on the sample plane, by focusing the femtosecond beam on the axon for 200ms.

Simultaneous imaging of the process of axotomy could be preformed using a) three channel confocal fluorescence imaging and (b) laser scanning brightfield imaging using the diascopic detector of the confocal laser scanning system (referred to as Confocal Laser Scanning Bright Field (CLSBF) hence forth). This allowed us to have simultaneously four images from the real time imaging process (blue, green, red and brightfield channels of the confocal microscope), either separately or aleatory combined. Multicolored acquisition was also facilitated by the presence of seven excitation wavelengths (that could be used simultaneously) provided by the confocal laser bed.

7.3.3 Damage assessment of surrounding tissue

In addition to real time observation of the laser nanosurgery procedure (by CLSBF and confocal fluorescence microscopy), and in order to aid us with the determination of the effectiveness of the axotomy procedure, all the available imaging techniques in the workstation were used to visualize the collateral damage in the vicinity structures or tissues. The parameters considered in evaluating collateral damage were a) increased autofluorescence in the surrounding tissue, b) damage to the muscle tissue just below the targeted neuronal commissure and c) damage to cuticle just above the targeted neuronal commissure.

Increased autofluorescence was observed using real time confocal fluorescence microscopy along with the process of surgery and two photon excited fluorescence microscopy performed post-surgically. Possible muscular damage was evaluated using Second Harmonic Generation (SHG) Microscopy performed post-surgically and using confocal florescence imaging simultaneously with surgery in case of fluorescently labeled muscle. Finally possible cuticle damage was evaluated using CLSBF performed simultaneously with neurosurgery and Multiphoton Laser Scanning Brightfield (MLSBF) imaging performed post surgically.

In all the operated worms the areas surrounding the neuron cut were imaged in real time using confocal microscopy and CLSBF. Post-Surgically several image stacks (from the cuticle surface to the midline of the worm) were taken using the same system to make a methodical screening of the areas in question. Images from the different channels were stored in separate files. Subsequently the same region was subjected to multiphoton imaging using TPEF, SHG and MLSBF imaging.

For the SHG imaging of the body wall muscles and cuticle, a series of ten images per stack were taken. This data was averaged and smoothed using Image-J 1.4 [224]. Visual observation of these images were done post image treatment in order to try to find the smallest resolved collateral damage.

The following imaging tools were used to make a through assessment of collateral damage during the process of nanosurgery. a) Confocal Laser Scanning Brightfield (CLSBF) imaging, b) confocal fluorescence imaging, c) Two Photon Excited Fluorescence (TPEF) microscopy, Second Harmonic Generation (SHG) imaging and Multiphoton Laser Scanning Bright Field (MLSBF) imaging. Before the start of surgical process the region around the point to be incised is imaged using MLSBF, TPEF and SHG multimodal imaging. Time

lapse (fastest possible by the system) Confocal florescence imaging (using at least two excitation wavelengths and 3 color detection) and CLSBF imaging was performed on the same focal plane as the plane of surgery, in real time during the process of surgery to image dynamic processes and also to detect possible collateral damage. Immediately after this the region was again imaged using TPEF, MLSBF and SHG multimodal microscopy. This was followed by obtaining image stacks at different focal planes using the confocal system to determine any possible collateral damage in planes other than the plane at which surgery is performed. The post-surgical TPEF, MLSBF and SHG multimodal imaging process is also repeated in different focal planes to better investigate possible collateral damage.

7.4 Dynamic processes during nano-Neurosurgery

A number dynamic processes were observed when the procedure of Nano-neurosurgery was observed live using 3 channel confocal microscopy and CLSBF imaging. These were 1) Spreading of autofluorescence in a single muscle cell, 2) GFP spilling, 3) Cavitation bubble opening a hole in the cuticle, 4) Cavitation bubble displacing the axon, 5) Muscular contraction and 6) Destruction of the whole axon. These active processes can take from few milliseconds (such as the GFP spilling that occurs promptly) to few tens of seconds. In Table 7.1 a summary of the above mentioned observed dynamics, the technique used to image the process, an approximate duration of the process, number of observed cases and reference to illustrations of the processes can be found.

Table 7.1: Dynamic processes during Nano-neurosurgery. CF:Confocal Fluorescence Microscopy, CLSBF: Confocal Laser Scanning Bright Field Microscopy, 2PE: Two Photon Excited Fluorescence Microscopy.

Observed dynamic effect	Imaging technique used	Duration of the effect	n (out of 90 trials)	Illustrations
Increased autofluorescence (damage)	CF, 2PE	Immediate upto 5s	60	Figure 7.14
Spreading of autofluorescence in single muscle cell	CF, 2PE	Immediate upto few seconds	12	Figure 7.2
GFP spilling	CF	Immediate up to 30s	16	Figure 7.3
Cuticle elasticity	CLSBF	Immediate up to 15s	12	Figure 7.4
Axonal displacement	CF	Immediate up to 15s	4	Figure 7.5 and 7.6
Muscular contraction	CLSBF, CF	Immediate up to 5s	29	Figure 7.7

7.4.1 Spreading of autofluorescence in a single muscle cell

An important effect that can be observed during nanosurgery is the spreading of green autofluorescence in a single muscle cell surrounding the point of impact of the laser scalpel. This is much unlike the autofluorescence that is observed as a result of collateral tissue damage, which is restricted to the immediate vicinity of the cut (See figure 7.14). The autofluorescence is confined to the muscle cell and does not spread to the neighboring sites. This is a dynamic process that takes place within a few seconds after the process of surgery and is usually irreversible.

Figure 7.1 shows the dynamics of the green autofluorescence increase in one of the operated worms. Impact of the laser beam severs the axon and also results in spreading of green autofluorescence in a single muscle cell below the point of surgery. Figure 7.1a shows the region before impact of the laser. Figures 7.1 b-1 shows the time lapse images as the autofluorescence spreads across the single muscle cell. The spreading reaches a steady state in about three seconds. The nucleus of the muscle cell does not show increased autofluorescence, and is seen as a dark region. Such increase in autofluorescence may indicate a collateral damage but this is not necessarily always the case.

Figure 7.2a shows another case where the impact of the laser does not sever the axon. Figure 7.2a shows the region before cut and Figures 7.2 b-l show the dynamics of the process. It can be seen that the green autofluorescence spreads across the entire muscle cell in about 8s. The boundary of the cell is clearly visible. In this particular case the axon is not severed and it seems the laser strikes a point slightly below the axon, on the muscle.

7.4.2 GFP Spilling

All neurosurgeries reported here were performed on neurons expressing GFP. Such neurons have a large concentration of GFP in their axoplasm. When the axon is severed the axoplasm spills out and is observed as dripping green droplets in real time confocal microscopy. Once such case is shown in Figure 7.3. Figure 7.3a shows the region before cut and Figures 7.3 b-l show the dynamics of the process. It can be seen that the impact of the laser severs the axon and immediately axoplasm starts spilling out. The droplets continue to fall out for about 15 seconds. It can also be observed that the impact of the laser also induces autofluorescence in one of the muscle cells. Such GFP spilling has been reported before in previous works on laser Nano-neurosurgery [216].

7.4.3 Cavitation bubble opening a hole in the cuticle

In case of femtosecond laser induced nanosurgery the point of energy deposition is well confined to the focal volume of the impacting laser beam . However the cavitation bubble formed as a result of this process happening in a liquid medium (biological sample) can sometimes propagate and create interesting effects. One of them is the creation of an opening in the cuticle. Cuticle being a collagenous elastic structure, the opening soon closes itself. This effect can be seen in Figure 7.4 where Figure 7.4a shows the CLSBF image of the midbody of the worm before the application of the femosecond laser beam for nanosurgery. The formation of the bubble opens up a hole (usually 2-3μm wide) in the cuticle immediately after the laser impact. The cuticle opening, however, closes back in a matter of few seconds. This is evidence of the elasticity of the collagen structure of the cuticle and can be an interesting phenomenon. Figure 7.4b shows the opening in

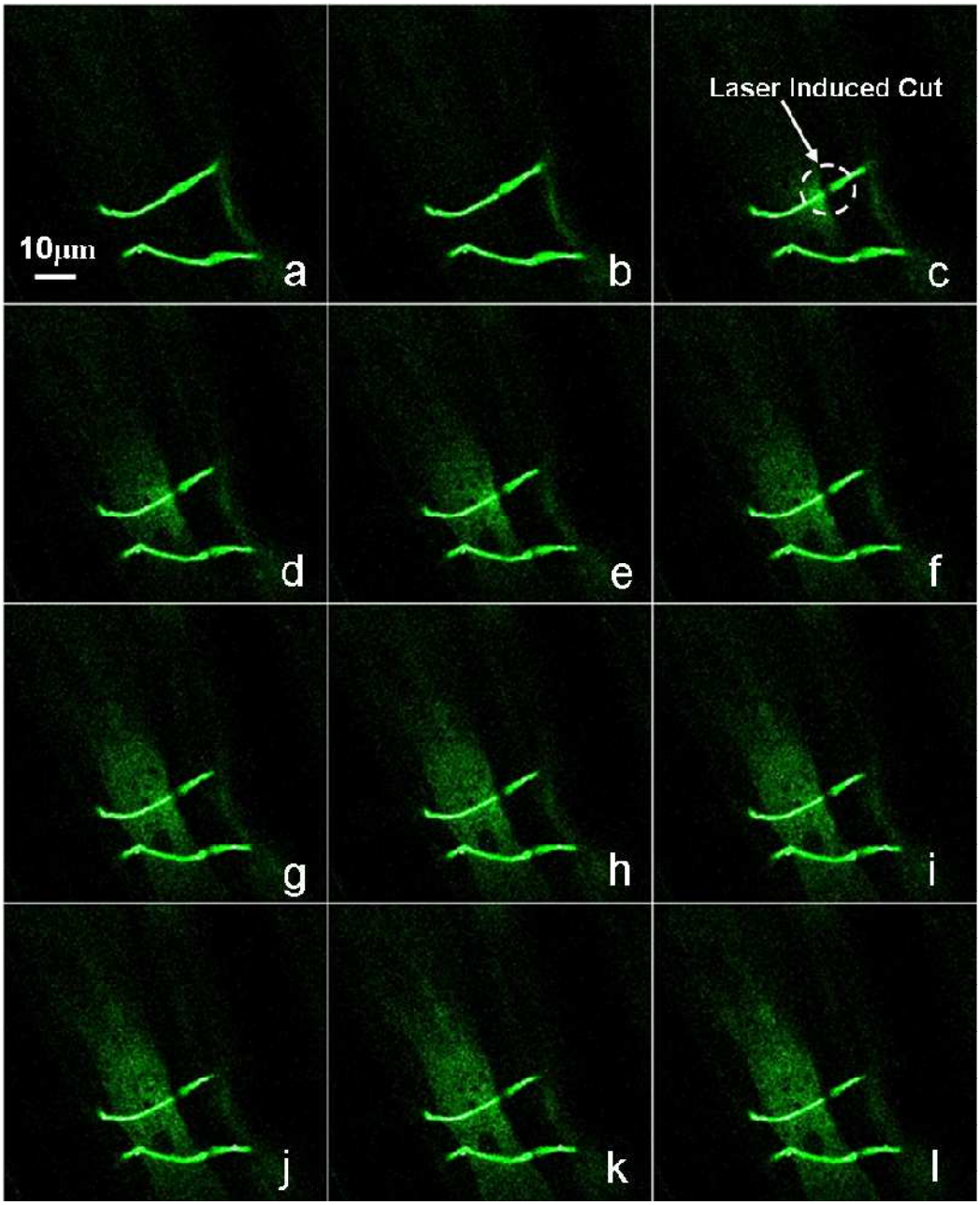

Figure 7.1: Time lapse images showing spreading of autofluorescence in a single muscle cell. a) Before cut. b-l) evolution of the autofluorescence after nanosurgery. Time between frames 1 second.

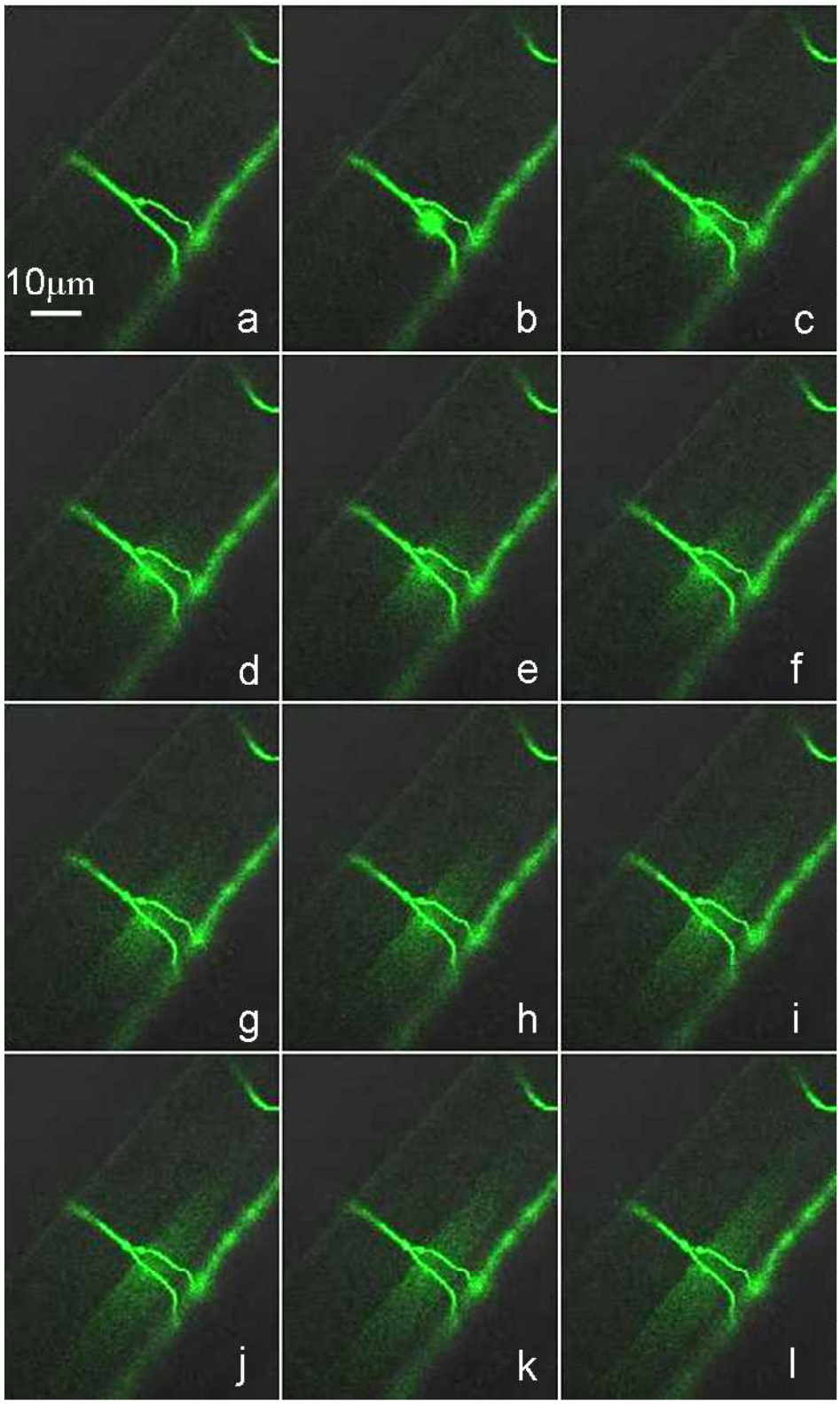

Figure 7.2: Time lapse images showing spreading of autofluorescence in a single muscle cell. a) Before cut; b-l) evolution of the autofluorescence in a single muscle cell after nanosurgery. Time between frames 1 second.

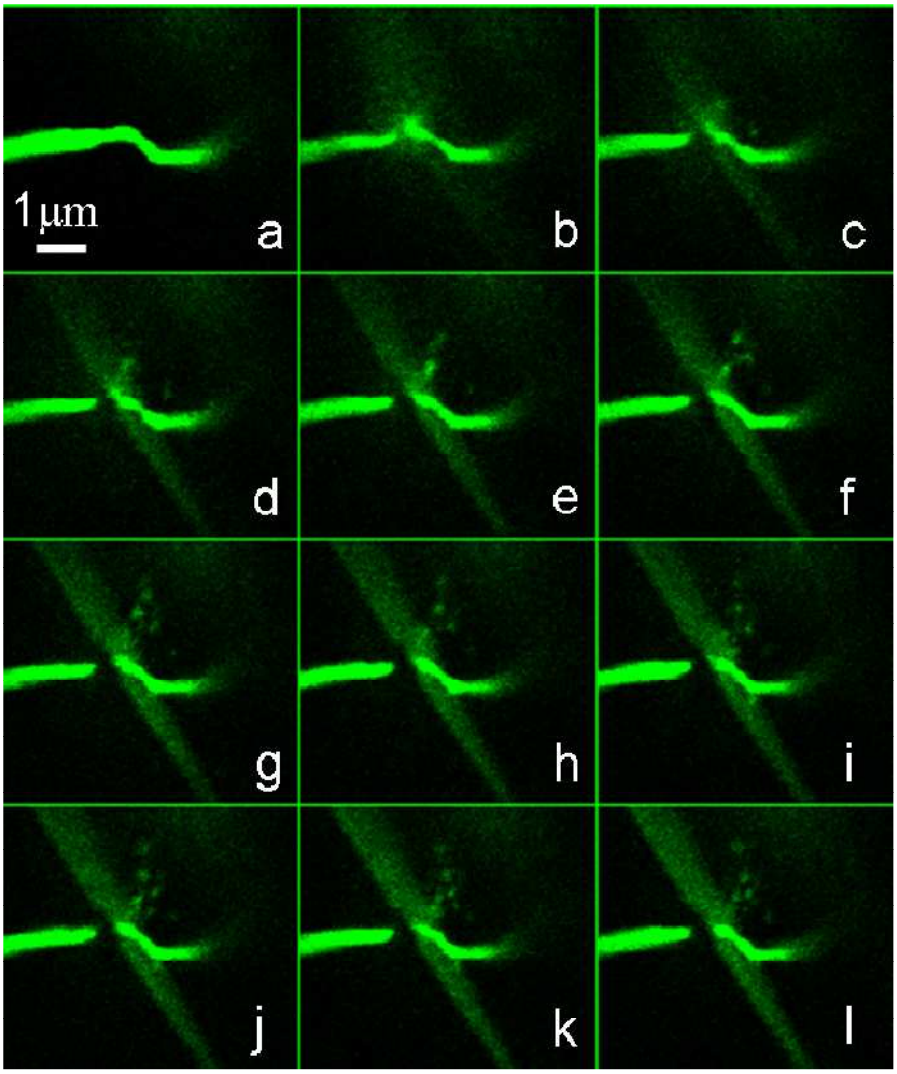

Figure 7.3: Time lapse images showing GFP expressing axoplasm spilling. a) Before cut; b-l) evolution of axoplasm spilling after nanosurgery; Time between frames 1 second.

the cuticle soon after the laser beam impacts on the neuron and severs the axon (axon severing not shown in the image). The hole closes down soon after (Figures 7.4 c-l). The time duration from the opening of the hole to its complete closure is about 8 seconds. This time can vary between a few seconds to about 15 seconds, depending on the operated case. Such opening of the cuticle by the cavitation bubble is seen only in 20% of the operated cases.

7.4.4 Cavitation bubble displacing the axon

It is sometimes observed that after the impact of the laser beam, the resulting cavitation bubble displaces the axon of the neuron aside and the axon is not severed. Soon after the displacement, the axon relaxes back more or less to its original position. This happens when the a slight error is committed in the target selection and the the laser beam focal spot impinges in a region slightly away from the axon. The axon stretches and relaxes back together with the opening created in the cuticle. This effect can be seen in Figure 7.5. Here Figure 7.5a shows the confocal fluorescence image of the neuron before the impact of the surgical laser beam. Figure 7.5b shows the stretching of the axon immediately after impact of the surgical laser spot. This axon relaxes back in about 12 seconds to almost its original state (Figures 7.5 c-o).

A more detailed picture of the effect can be seen in (Figure 7.6). The images are the superposition of the blue and green channels of the confocal microscope. It is interesting to observe a blue autofluorescence appear in the region where the cavitation bubble induces the aperture in the cuticle. The blue autofluorescence is observed when the sample is excited with a wavelength of 457nm in addition to the 488nm required for exciting the GFP in the neurons.

7.4.5 Muscular contraction

Interaction of the femtosecond laser spot with the muscle surrounding the axon can lead to muscular contraction. Such femtosecond induced muscular contraction has been reported in cardiomyocytes *in-vitro* [225]. However it is for the first time, to the best of our knowledge, that this effect has been demonstrated in the nematode *C.elegans*. The muscle contracts in a matter of few seconds after the impact of the laser beam and in another few seconds relaxes back. This effect can be observed in Figure 7.7. Figure 7.7a shows the CLSBF image of the midbody of the worm before surgery. Figures 7.7b-l show the progression of the process. To facilitate better observation of the effect the position of a prominent anatomical reference in the image has been marked using horizontal and vertical dashed lines. The displacement of the reference can be easily observed. Muscular contraction results in movement of the whole midbody. Contraction lasts about 4s and in about further 5 seconds the muscle relaxes back.

7.4.6 Destruction of the whole axon

It is rarely observed that the process of inducing a tiny incision in the axon using femtosecond laser axotomy induces an effect not just on the region of incision but also on the whole axon. These effects could be a result of the axon losing significant amount of material as a result of the loss of axoplasm through the region of incision. Figure 7.8, shows one such case. Figure 7.8a shows the TPEF image of the axon before surgery and Figure 7.8b shows the axon post surgery. It can be easily observed that the whole axon

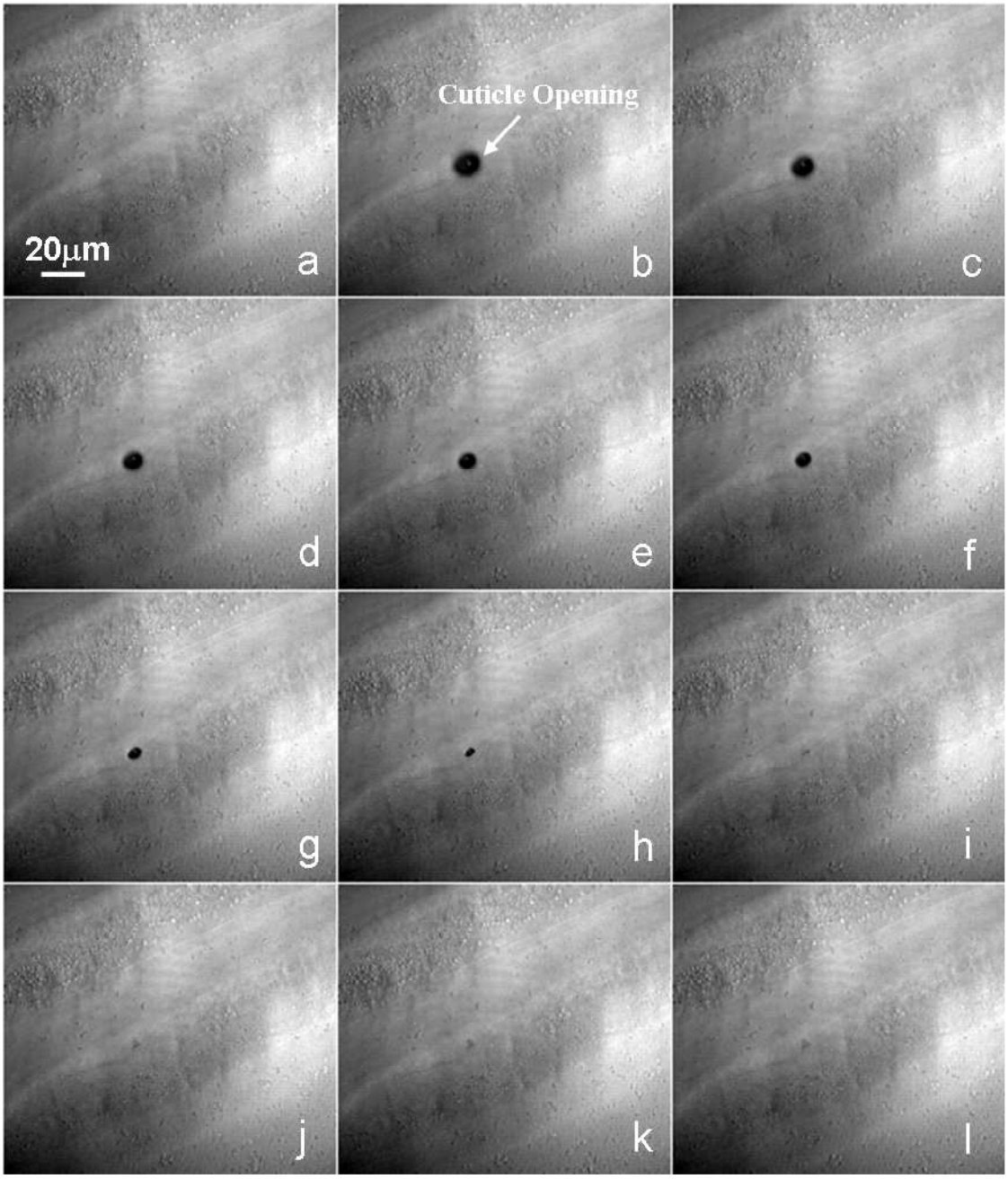

Figure 7.4: CLSBF time lapse images showing opening of the cuticle by the cavitation bubble. a) Before cut; b-l) evolution of cuticle opening closure. Time between frames 1 second.

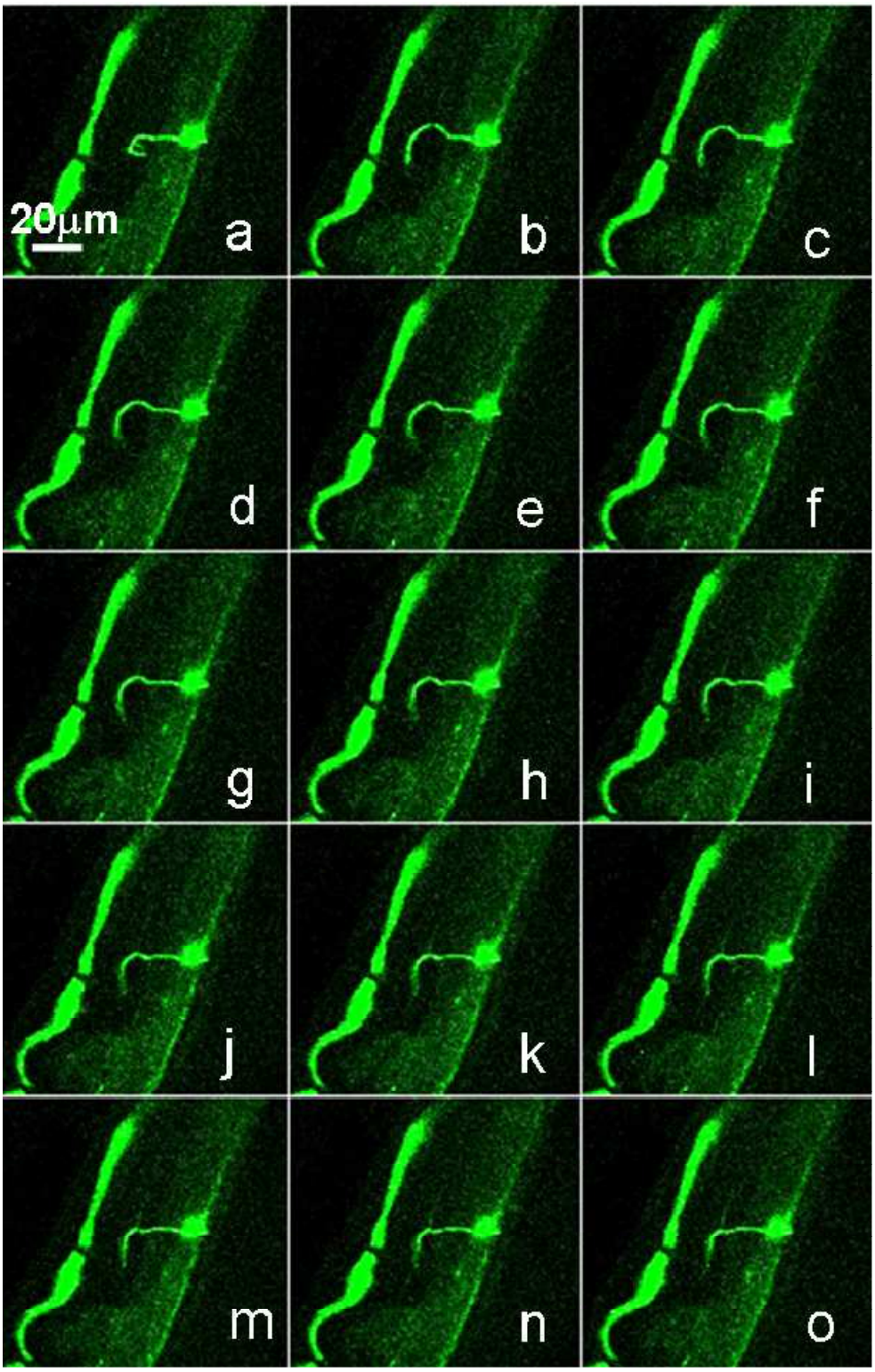

Figure 7.5: Time lapse confocal microscopy (green channel) images showing displacement of an axon by the cavitation bubble induced cuticle opening; a) Before cut; b-o) evolution of displacement. Time between frames 1 second.

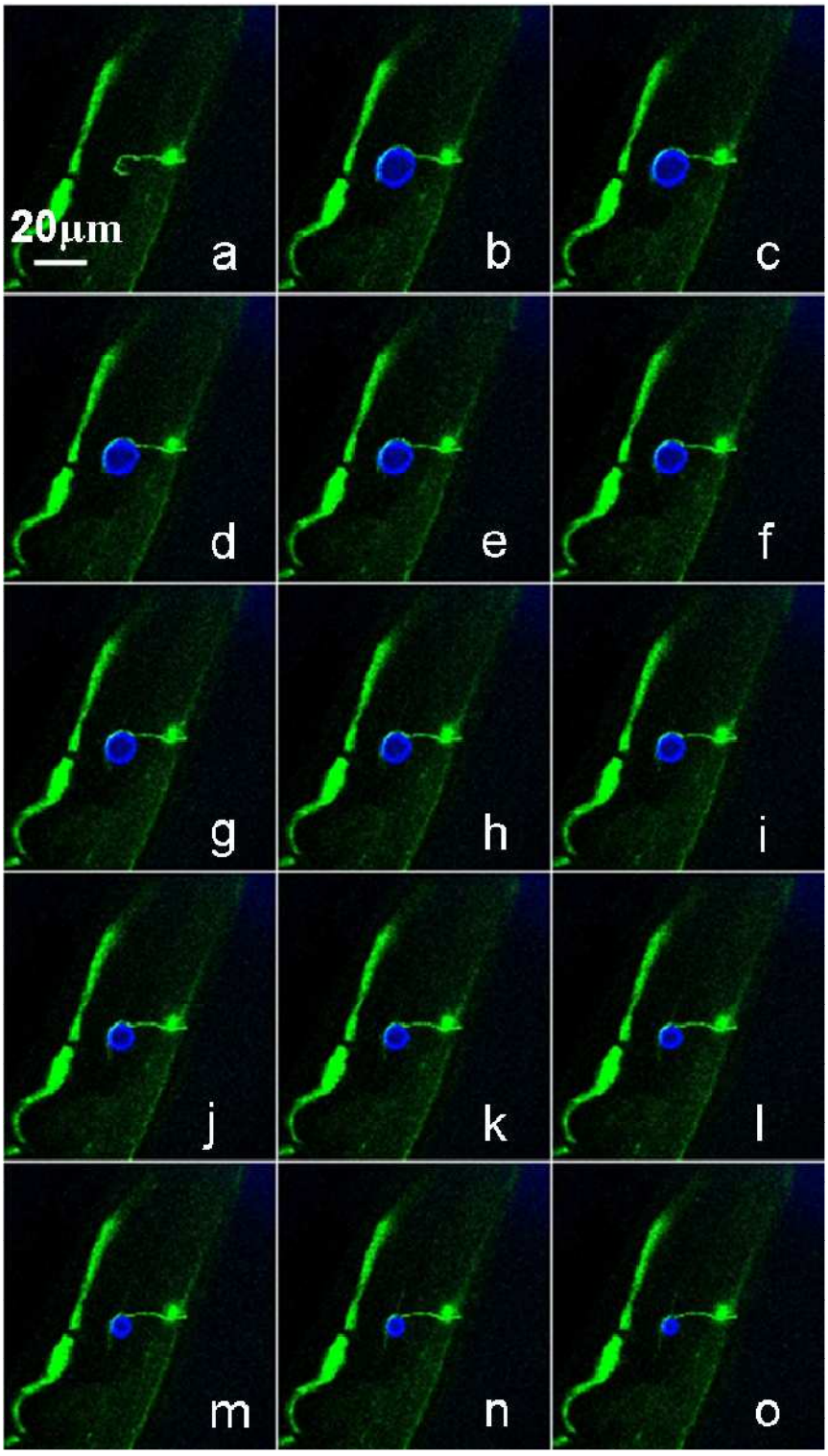

Figure 7.6: Time lapse images (combined blue and green channels) showing pushing aside of an axon by the cavitation bubble induced cuticle opening as well as the progression of the closure of the cuticle opening; a) Before cut; b-o) evolution of the push and opening in the cuticle. Time between frames 1 second.

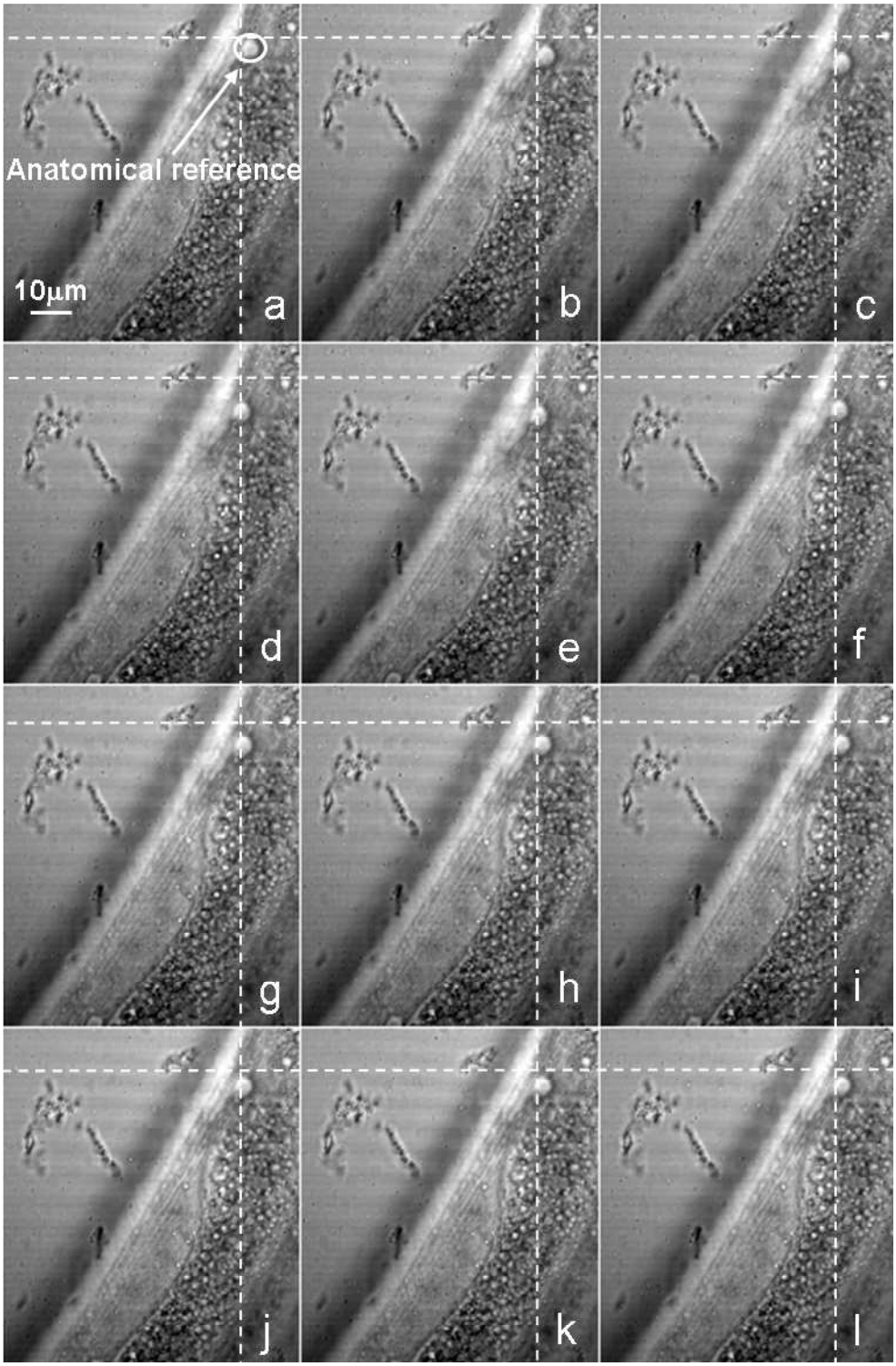

Figure 7.7: Time lapse LSBF images showing contraction of muscle as a result of impact of the laser beam on the muscle surrounding the axotomized neuron. a) Before cut; b-1) Time evolution of muscular contraction. Observation of a prominent anatomical reference whose position has been marked helps visualization of the process. The horizontal and vertical dashed lines help track the position of the anatomical reference. Time between frames 1 second.

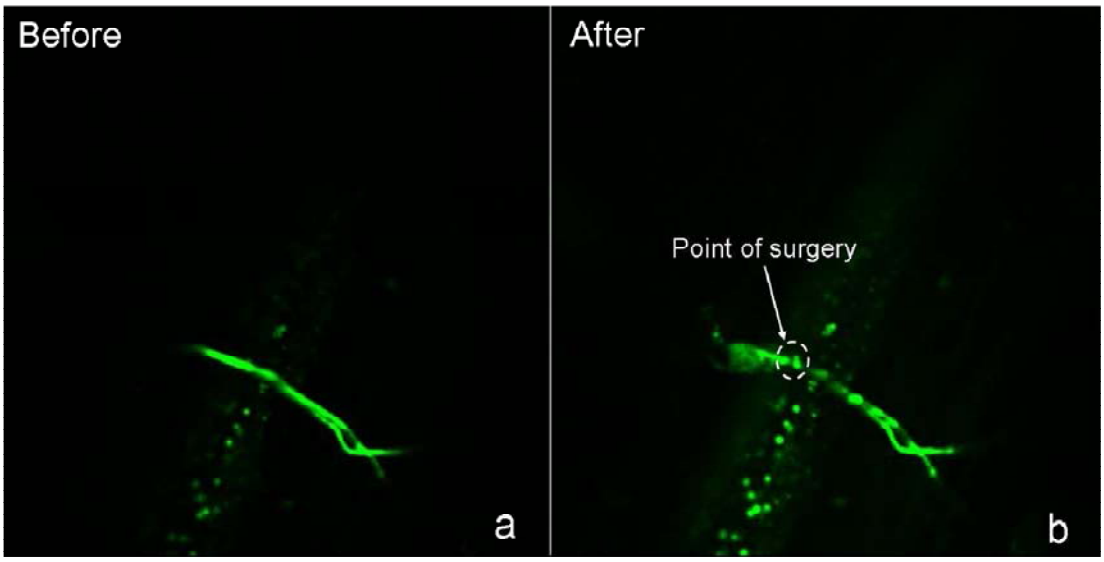

Figure 7.8: TPEF images showing destruction of the whole axon as a result of Nano-neurosurgery. a) Before cut; b) After cut

after surgery has undergone a structural change. There are a number of varicosities in the axon.

7.5 Collateral damage assessment

In this study various imaging modalities were used to assess collateral damage. Damage to tissue surrounding the commissure targeted for surgery was assessed using confocal fluorescence imaging performed live and TPEF imaging performed post-surgically. Damage to cuticle just above the targeted commissure was performed using CLSBF live and MLSBF post-surgically. Finally collateral damage to muscle just below the commissure was assessed using SHG microscopy performed post-surgically. Table 7.2 provides details of the numbers of different collateral damages detected and the sample size used to evaluate these.

Table 7.2: Collateral damage during Nano-neurosurgery observed using various imaging modalities. CF: Confocal Fluorescence Microscopy; 2PE: Two Photon Excited Fluorescence Microscopy; CLSBF: Confocal Laser Scanning Bright Field Imaging; MLSBF: Multiphoton Laser Scanning Bright Field Imaging; SHG: Second Harmonic Generation Microscopy; n: number of observed cases; N: sample size.

	Induced Autofluorescence (CF)	Induced Autofluorescence (2PE)	Cuticle Damage (CLSBF)	Cuticle (MLSBF)	Muscle damage (SHG)	YFP marked muscle
n	38	30	12	8	37	15
N	80	62	80	46	55	16

7.5.1 Collateral damage in muscle observed through SHG microscopy

SHG microscopy in the last few years has developed into a very powerful tool to look at muscle with its inherent advantage of not requiring any fluorophore [226]. SHG microscopy hence can reveal even minute collateral damages induced in the muscle as a result of the process of nanosurgery. The muscle in the region around the target neuron was imaged pre-surgically and post-surgically and these images were compared to detect any possible damage.

Figure 7.9 shows a case where post-surgically a very tiny damage in the form of a cut in the muscle was detected in the muscle cell just below the point of surgery. Figures 7.9 a, b and c respectively show the TPEF image of neurons, SHG image of muscle and a combination of these two image channels in the region of surgery before administration of the surgical incision. Figures 7.9 d, e and f respectively show the TPEF image of neurons, SHG image of muscle and a combination of these two image channels in the region of surgery after administration of the surgical procedure. The impact of the laser scalpel severs the axon and also creates a minute damage in the muscle. This damage would have gone unnoticed without the use of SHG microscopy, since there is no induced autofluorescence detected in the TPEF image or the confocal fluorescence images (data not shown) acquired in real time with the process of surgery.

Figure 7.10 shows a case where there is a prefect incision created in the axon without any collateral damage detected what so ever (no induced autofluorescence detected using TPEF (Figure 7.10d) and confocal fluorescence), no cuticle damage detected in CLSBF and MLSBF (data not shown) and no muscle damage detected using SHG microscopy (7.10e)). In this case the target on the commissure for nanosurgery was selected in a region between the muscle cells to avoid any possible collateral damage to the muscle.

With accurate selection of the focal plane of the point of surgery and tight control over various optical parameters, even with the use of high repetition rate (100MHz) femtosecond laser, very precise incisions without any collateral damage can be performed. One such case is shown in Figure 7.11 were an incision is made on a commissure section which is just above a muscle cell and there is no collateral damage in the muscle as observed through SHG microscopy (Figure 7.11e). It may be noted that the muscle cell is just a few hundred nanometers below the commissure targeted for surgery. There was no damage to the cuticle as observed through CLSBF and MLSBF imaging (data not shown). There was also no induced autofluorescence as observed through TPEF microscopy (Figure 7.11d) performed post surgically and confocal fluorescence microscopy performed live.

Some times the damage to the muscle does not result in a cut in the muscle but induces a wave like pattern in the muscle cell in a region just adjacent to the incision in the axon. Such a case is shown in Figure 7.12. An induced autofluorescence in a single muscle cell is also observed (Figure 7.12e) . The wavelike pattern may be induced because of the laser induced muscular contraction and incomplete subsequent relaxation in that region which has undergone a slight collateral damage.

There are also cases where collateral damage to the muscle is so tiny that it manifests only as a small reduction in the SHG signal coming from that region. SHG signal is very much dependent on the microscopic structural organization in the sample [226]. It is very well possible that the effect of collateral damage was not sufficient to induce a cut in the muscle but sufficient enough to cause a disorganization on the microscopic arrangement

of harmonophores which results in a reduction of SHG signal. Such a case is shown in Figure 7.13.

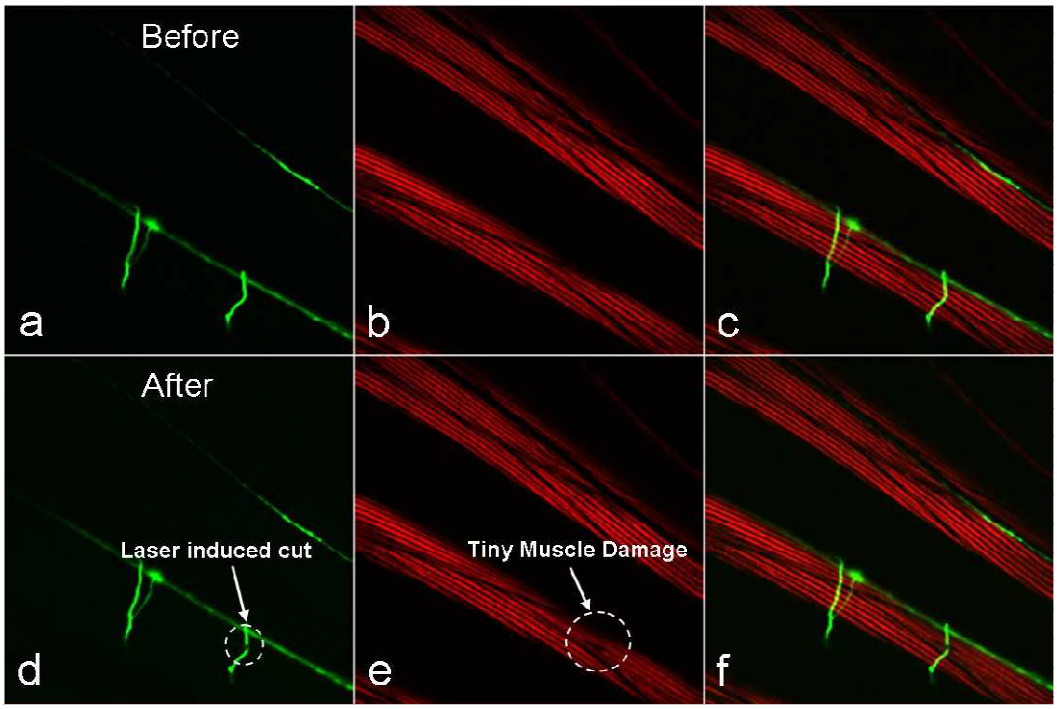

Figure 7.9: A tiny damage detected in muscle after the Nano-neurosurgery procedure. a) TPEF image before cut; b) SHG image before cut; c) Combined TPEF and SHG image before cut; d) TPEF image after cut; e) SHG image after cut; f) Combined TPEF and SHG image after cut

7.5.2 Multimodal imaging to detect collateral damage induced by the process of Nano-neurosurgery

Multimodal imaging was performed as described in section 7.3.3 to make a through and complete assessment of collateral damage, with all the available tools in the multimodal optical workstation.

Figure 7.14 shows collateral damage detected in one of the operated cases using confocal fluorescence imaging and CLSBF imaging when imaged live during the process of Nano-neurosurgery. Figures 7.14 a,b and c respectively show the confocal fluorescence image of the targeted neuron, CLSBF image of the corresponding body of the worm and a superposition of these two images before performing the surgical procedure. Figures 7.14 d,e and f, respectively, show the confocal fluorescence image of the targeted neuron, CLSBF image of the corresponding body of the worm and a superposition of these two images after performing the surgical procedure. A hole can be detected in the confocal fluorescence image after administration of the surgical procedure. Moreover the region around the hole shows increased green autofluorescence. Cuticle damage can be observed in the CLSBF image. Figure 7.14 also brings out the difference between autofluorescence increase due

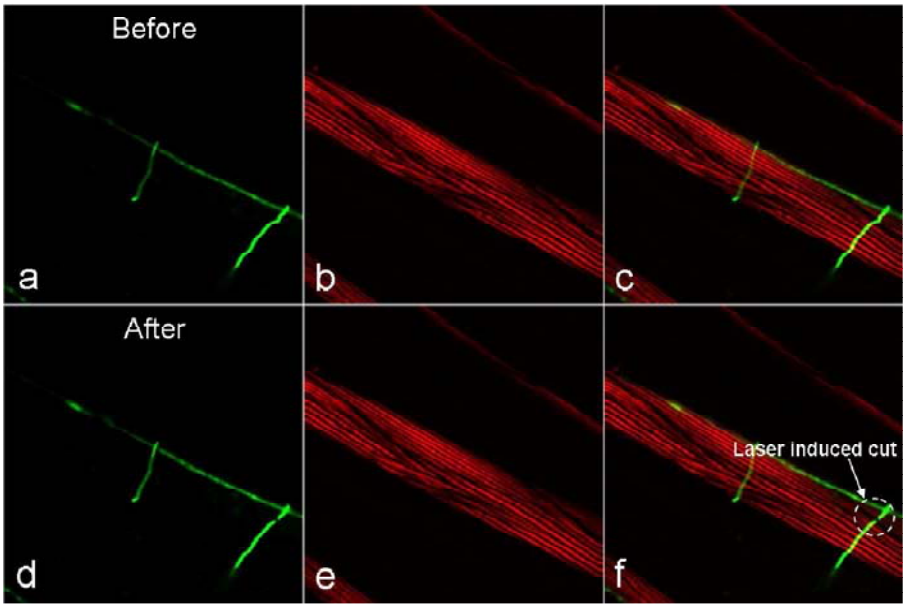

Figure 7.10: Nanosurgery performed without any collateral muscle damage. a) TPEF image before cut; b) SHG image before cut; c) Combined TPEF and SHG image before cut; d) TPEF image after cut; e) SHG image after cut; f) Combined TPEF and SHG image after cut

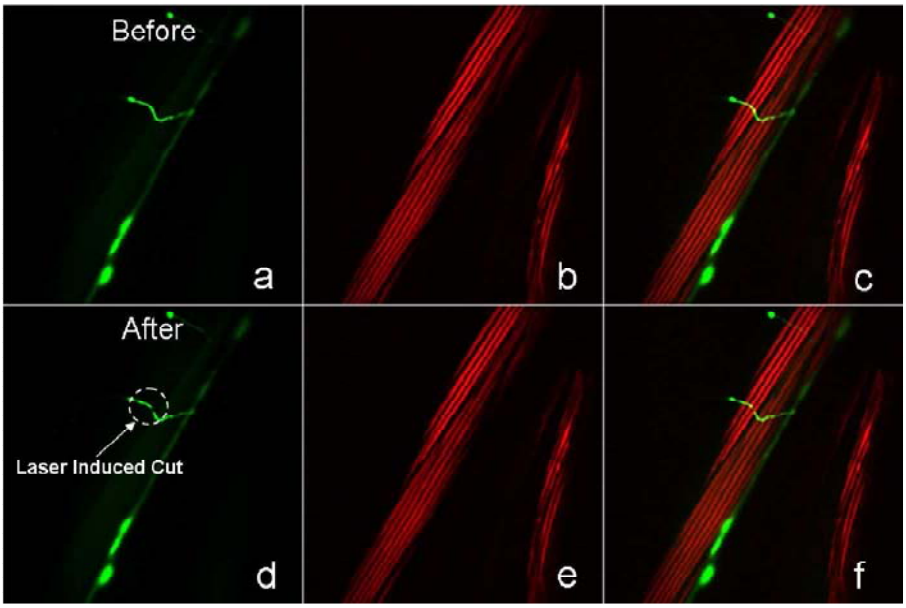

Figure 7.11: Nano-neurosurgery performed without any collateral muscle damage. a) TPEF image before cut; b) SHG image before cut; c) Combined TPEF and SHG image before cut; d) TPEF image after cut; e) SHG image after cut; f) Combined TPEF and SHG image after cut

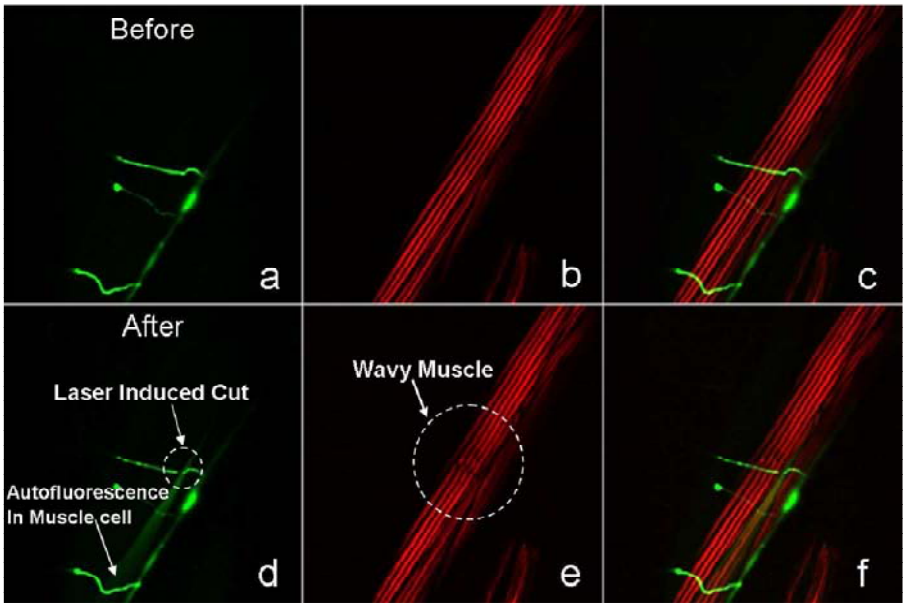

Figure 7.12: Nano-neurosurgery induces a wavy pattern in the muscle. a) TPEF image before cut; b) SHG image before cut; c) Combined TPEF and SHG image before cut; d) TPEF image after cut; e) SHG image after cut; f) Combined TPEF and SHG image after cut

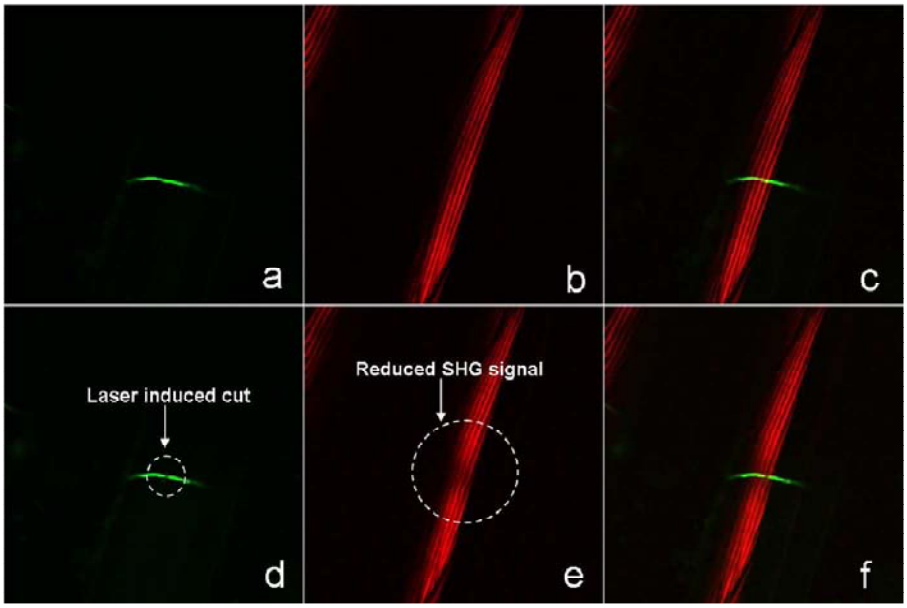

Figure 7.13: Nano-neurosurgery induces a reduction in the SHG signal. a) TPEF image before cut; b) SHG image before cut; c) Combined TPEF and SHG image before cut; d) TPEF image after cut; e) SHG image after cut; f) Combined TPEF and SHG image after cut

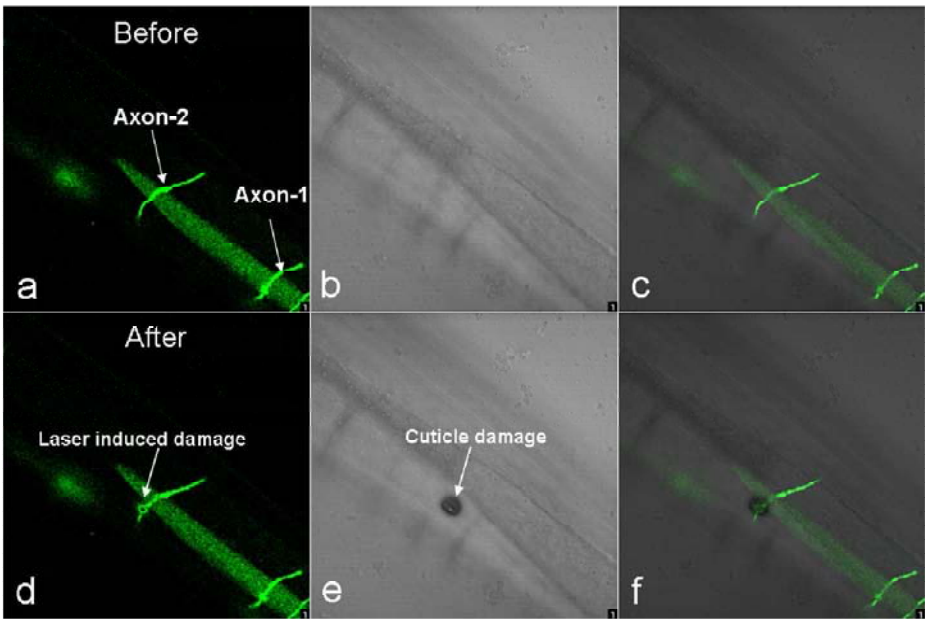

Figure 7.14: Confocal multimodal imaging of Nano-neurosurgery where the process induces collateral damage. a) Confocal fluorescence image of neurons before cut b) Confocal LSBF image of the body before cut; c) Combined confocal fluorescence and LSBF image before cut; d) Confocal fluorescence image of neurons after cut; e) Confocal LSBF image of the body after cut; f) Combined confocal fluorescence and LSBF after cut

to collateral damage and autofluorescence spreading in a single muscle cell as a result of muscular stimulation. Axon-1 was incised before axon-2 (Figure 7.14a) and it resulted in spreading of green autofluorescence in the muscle cell just below it. The cell boundary is clearly visible. Incision on axon-2 (Figure 7.14d) resulted in collateral damage and increased autofluorescence around the point of incision in the form of a circle of diameter around 1μm.

Multimodal multiphoton imaging was performed on the same worm in the same region as in Figure 7.14. This is shown in Figure 7.15, which shows collateral damage detected in TPEF imaging, SHG imaging as well as MLSBF imaging performed post-surgically. Figures 7.15 a,b and c, respectively, show the TPEF image of the targeted neuron, SHG image of the corresponding muscle and a MLSBF of the corresponding body region of the worm before performing the surgical procedure. The surgical process results in collateral damage. Figures 7.15 d, e and f, respectively, show the TPEF image of the targeted neuron, SHG image of the corresponding muscle and a MLSBF of the corresponding body region of the worm after performing the surgical procedure. The region around the hole shows increased green autofluorescence in the post-surgical TPEF image. A cut in the muscle is detected in the post surgical SHG image and cuticle damage can be observed again in the MLSBF image. Both confocal (Figure 7.14) and multiphoton imaging (Figure 7.15) reveals collateral damage in this case.

In many cases no damage is detected in live confocal fluorescence imaging and CLSBF imaging while post surgical SHG imaging detects muscular damage. One such case is

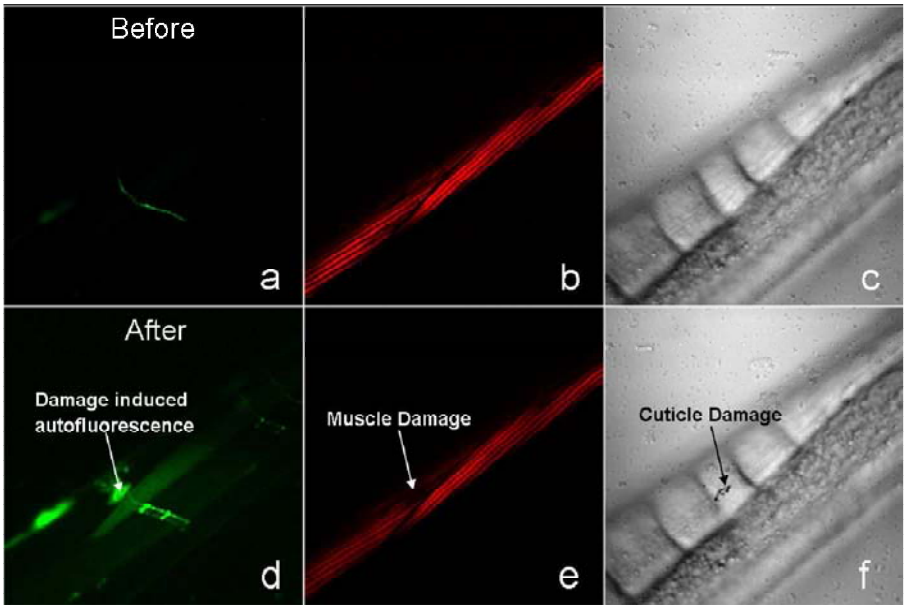

Figure 7.15: Nano-neurosurgery induces collateral damage. Multiphoton imaging corresponding to Figure 7.14. a) TPEF image before cut; b) SHG image before cut; c) LSBF image before cut; d) TPEF image after cut; e) SHG image after cut; f) LSBF image after cut

shown in Figure 7.16. Figures 7.16 a, b and c respectively show the confocal fluorescence image of the targeted neuron, CLSBF image of the corresponding body of the worm and a superposition of these two images before performing the surgical procedure. Figures 7.16 d, e and f respectively show the confocal fluorescence image of the targeted neuron, CLSBF image of the corresponding body of the worm and a superposition of these two images after performing the surgical procedure. No damage can be detected either in the form of induced autofluorescence in the confocal fluorescence image or cuticle damage in the CLSBF image.

However post-surgical SHG imaging reveals a tiny damage in the muscle as seen in Figure 7.16. Figures 7.16 g, h and i respectively show the TPEF image of the targeted neuron, SHG image of the corresponding muscle and a superposition of TPEF and SHG images before performing the surgical procedure. Figures 7.16 j, k and l respectively show the TPEF image of the targeted neuron, SHG image of the corresponding muscle and a superposition of TPEF and SHG images after performing the surgical procedure. The post-surgical TPEF image does not show any induced autofluorescence, however the post-surgical SHG image shows a tiny damage in the muscle.

There have also been few cases where there is no damage detected in the live confocal fluorescence and CLSBF imaging and post surgical TPEF, MLSBF and SHG imaging in the same plane as the point of surgery. However SHG imaging in planes different from the point of surgery reveals small amounts of muscular damage. One such case is shown in Figure 7.17. Here Figures 7.17 a,b and c respectively show the TPEF image of the targeted neuron, SHG image of the corresponding muscle and a superposition of the TPEF and SHG images before performing the surgical procedure. Figures 7.17 d,e and

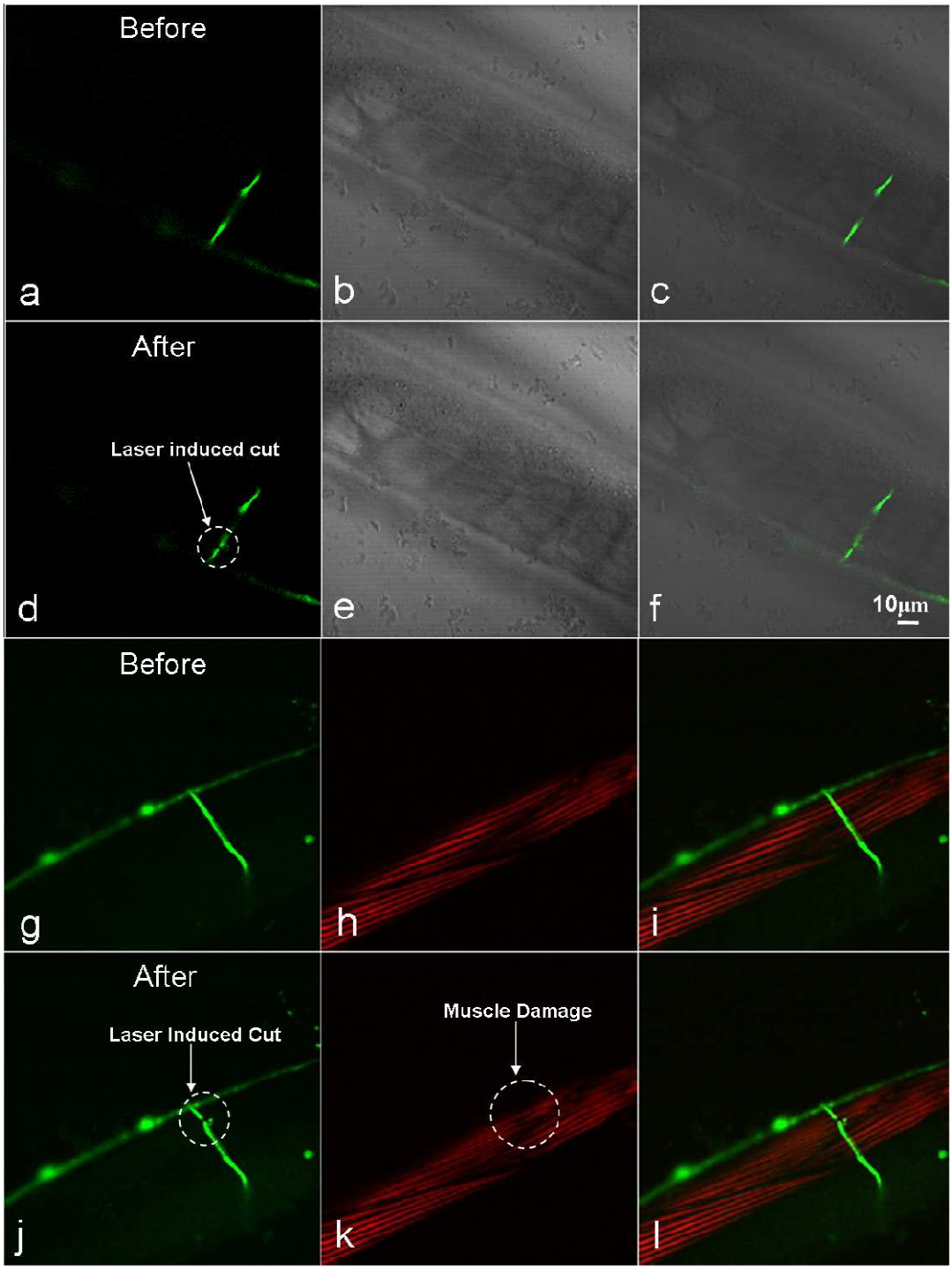

Figure 7.16: No collateral damage observed in Confocal multimodal imaging while damage observed in SHG microscopy of muscle. a) Confocal fluorescence image before cut; b) confocal LSBF image before cut; c) Combined confocal fluorescence and LSBF image before cut; d) Confocal fluorescence image of neurons after cut; e) Confocal LSBF image of the body after cut; f) Combined confocal fluorescence and LSBF after cut g) TPEF image before cut; h) SHG image before cut; i) Combined TPEF and SHG image before cut; j) TPEF image after cut; k) SHG image after cut; l) Combined TPEF and SHG image after cut.

f show the same, in the same plane as the plane of the point of surgery after performing the surgical procedure. No damage is detected in these images. However Figures g,h and i which respectively show the TPEF image of the targeted neuron, SHG image of the corresponding muscle and a superposition of the TPEF and SHG images in a plane slightly below the plane of the point of surgery after performing the surgical procedure shows some amount of damage. Even though some muscle damage might also be observed in Figure 7.17e, the damage is more prominently visible in Figure 7.17h.

7.5.3 Damage assessment using strains with fluorescently labeled muscle

Collateral damage to muscle during the process of Nano-neurosurgery can also be detected using live confocal fluorescence microscopy using *C.elegans* strains which have their muscles tagged with a fluorescent label. One such strain with bodywall muscles fluorescently tagged with YFP was used in the present study. Figure 7.18 shows a case where the collateral damage in muscle during the neurosurgical process has been detected by imaging the YFP tagged muscle. The images are the superposition of the blue and green channel of the confocal microscope. Figure 7.18a, shows the axon and the surrounding muscle before the surgical process. Figure 7.18b, shows the axon and the surrounding muscle during the impact of the femtosecond beam focus on the target. The impact of the laser beam severs the axon, induces a small damage in the muscle as well as blinds the confocal detectors for a moment. The result of the blinding of the confocal detectors is seen as a strip in Figure 7.18b. Blue autofluorescence due to cavitation bubble induced cuticle opening effect is also seen. The blue autofluorescence however diminishes very quickly in about 2 seconds. Figures 7.18 c-l shows the progression of the dynamics which also includes muscular contraction.

7.6 Discussion

Laser axotomy was preformed in D-type axons in *C.elegans* using MHz femtosecond laser and real time imaging of the process was done with single photon fluorescence imaging and laser scanning brightfield imaging. More than 50 laser cuts of neuronal axons were made by placing a static femtosecond beam on the targeted area for an exposure time of 200ms. All the cuts were visualized in real time.

Post surgery imaging of the targeted and surrounding regions was done using both linear and nonlinear imaging techniques. The combination of all these high resolution imaging tools showed a great importance/significance not only to the study of the process of laser cutting itself, but also to be able to perfect the technique of laser nanosurgery by assessing the development of the cut and to study the possible inflicted collateral damage.

Real time imaging of the Nano-neurosurgery procedure revealed a number of dynamics such as: GFP spilling from the axon tips, opening and closure of elastic cuticle, worm muscular reaction to laser and immediate damage of the surrounding areas with induced autofluorescence etc:. In addition real time imaging also reveals if the axon has been severed. This is quite often a problem when looking only at the images post-surgically, since it is difficult to determine if the region of attempted incision really shows a severing or if it is only photo bleaching. The dynamics of the procedure when observed in real time

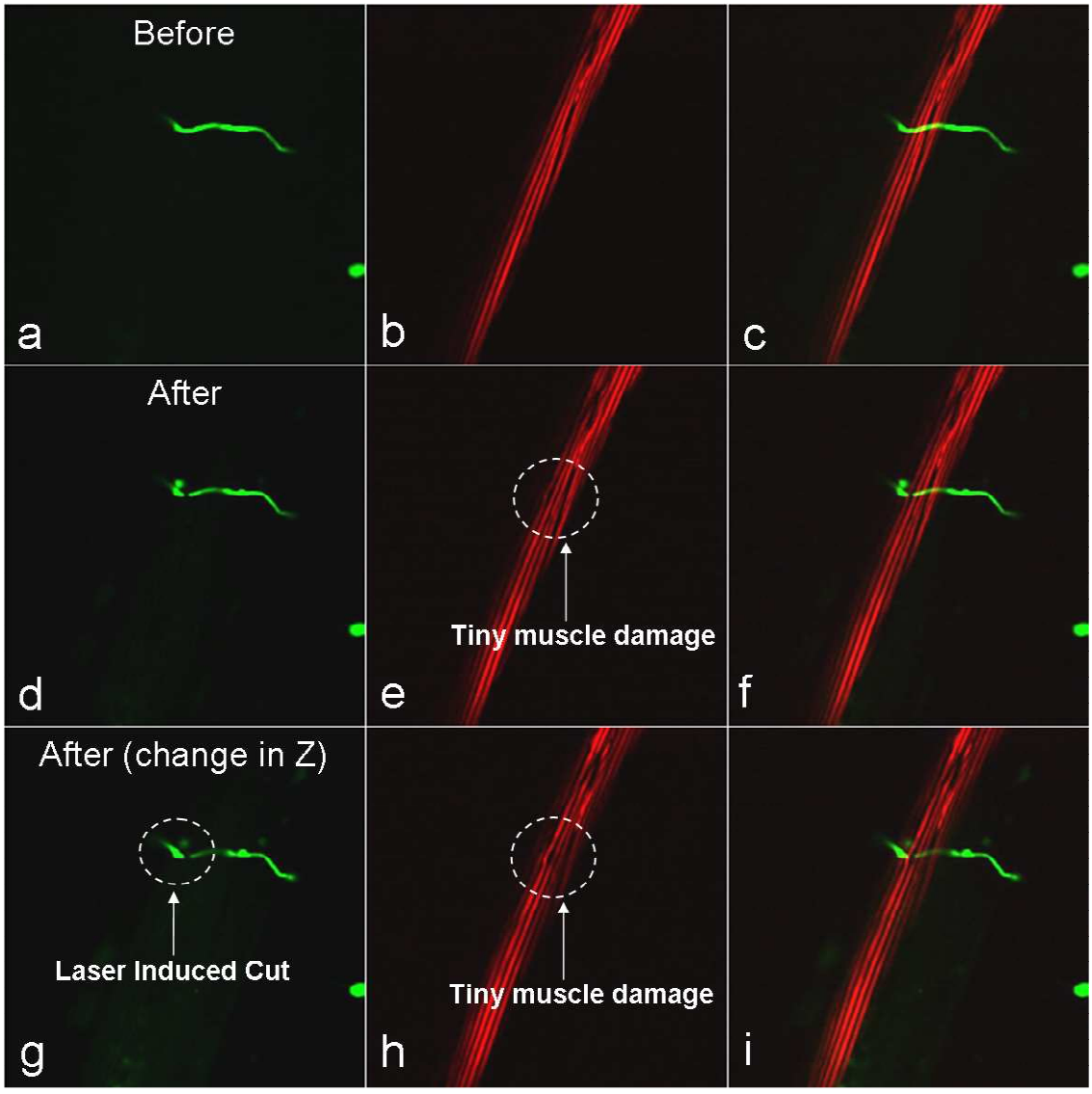

Figure 7.17: Collateral damage better observed after multiphoton imaging in different planes. Collateral damage is observed only in the SHG image of muscle. a) TPEF image before cut; b) SHG image before cut; c) Combined TPEF and SHG image before cut; d) TPEF image after cut; e) SHG image after cut; f) Combined TPEF and SHG image after cut; g) TPEF image after cut in a plane below the cut; h) SHG image after cut in a plane below the cut; i) Combined TPEF and SHG image after cut in a plane below the cut.

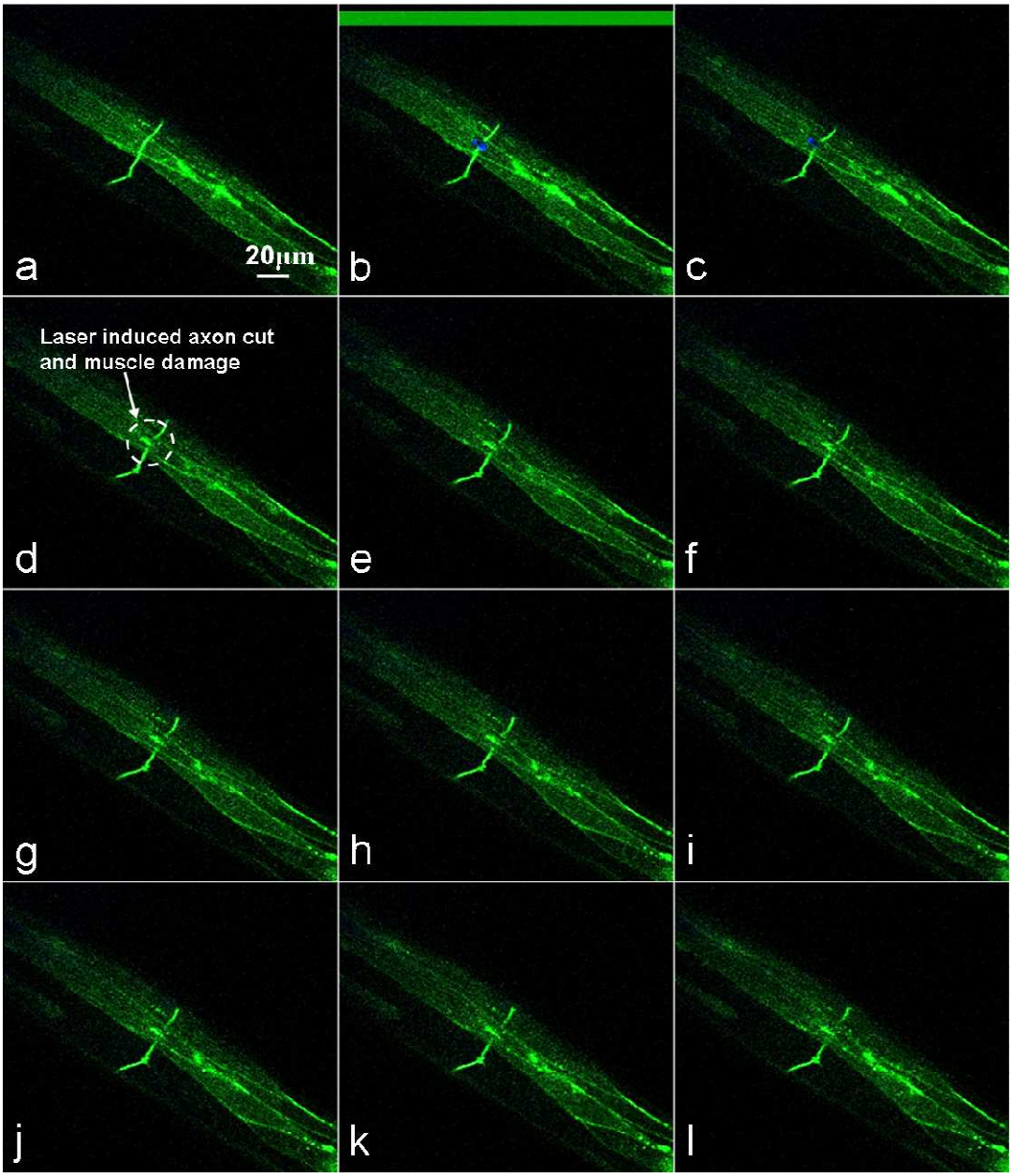

Figure 7.18: Collateral damage to muscle during Nano-neurosurgery detected using YFP labeling in the muscle. a) Before cut; b-l) Dynamics of the evolution of the laser induced cut and related processes.

is very different (data not shown) if the laser has only managed to photobleach the sample than when it has actually severed the commissure.

This multimodal workstation allowed, within others, the nano-manipulation of the axons in *C. elegans* and real time imaging with different techniques. With the use of the presented multimodal workstation, and more specifically with a femtosecond laser nanosurgery scalpel simultaneously used with single photon imaging, many dynamic phenomena that occur during laser nanosurgery were revealed, to our knowledge, for the first time. Some of these dynamic phenomena, and their impact in the collateral damage assessment of the resulting operated worm, would have been missed out of observation if simultaneous imaging was not used.

Among the many observed dynamic effects, a very interesting observation was the laser induced muscular contraction. This happens when there is a slight interaction between the femtosecond laser spot with the muscles surrounding of axonal areas, while the laser impacts the axon. Femtosecond laser induced muscular contraction has been reported in cardiomyocytes *in-vitro* [225]. It has been demonstrated that by periodic exposure to femtosecond laser pulse-trains, periodic contraction cycles in cardiomyocytes could be triggered, depleted, and synchronized with the laser periodicity. Muscle contraction is a calcium signaling dependent process. The calcium ions bind and interact with molecules associated with the cells contractile machinery, the end result being a mechanical contraction. Any means that can induce elevations in calcium ions can as a result induce muscular contraction. Femtosecond laser irradiation is one of these means and can possibly induce muscular contraction.

Femtosecond laser induced cavitation bubbles and their effect in the sample has been thoroughly predicted and assessed by Vogel [84]. The occurrence of the cavitation bubbles may result in inherent damage that can be due to dissociation of biomolecules into volatile non-condensable fragments. The cavitation bubble opens up a hole in the cuticle in many operated cases, which closes back in a few seconds. The observation of this phenomenon discloses some of the worms anatomical characteristics that might be of interest to investigate such as the elasticity of the neuronal processes, cuticle and muscular cells. In most of these cases there is apparently no damage in the post surgery observation to any structure including the cuticle where the hole opened.

The emergence of increased autofluorescence in the surrounding areas of the laser surgery is also a phenomenon that has been reported before [84]. This usually indicates damage is mainly due to mitochondria destruction at the edge of the laser incision. GFP spilling from the severed axon tips has also been observed before by epi- fluorescence microscopy (Frederic Bourgeois and Adela Ben-Yakar [216]. Nevertheless, not much information on the process is known.

One other highly appealing subject of future work is the observed spreading of autofluorescence in a single muscular cell after laser impact in the vicinity of the muscle cell. There seems to be laser stimulation of a single cell where a wave of autofluorescence spreads in few seconds through the cell with exception to the cell nucleus. Such increase of intrinsic fluorescence could be explained as a result muscle stimulation and resulting NAD(P)H increasing autofluorescence. There are many factors that can fuel cell NAD(P)H levels such as workload, dehydrogenase activity, and cytosolic-mitochondria compartmentalization and, therefore, the interpretation of NAD(P)H fluorescence in intact tissues must be mindful. Nonetheless, single cell muscular stimulation and NAD(P)H increased autofluo-

rescence due to mitochondrial metabolism in contracting cells [227] can be a potentially strong explanation. This subject certainly deserves further study.

A combination of linear imaging techniques used in real time along with the process of surgery as well as non-linear imaging techniques performed post surgically were used to make a through detection of collateral damage during the process of Nano-neurosurgery. Collateral damage to muscle, cuticle and other surrounding structures could be detected using these high resolution imaging techniques.

Cuticle and muscle lie in very close proximity (within a micrometer) to the D-type motor neurons and ability to target the axon without damaging these structures requires the laser beam to be spot on and to deliver its destructive effects well within one micrometer. Studies of damage to cuticle and muscle hence provides a very rigorousness assessment of the quality of the surgery tool. Even a very small error would show up as collateral damage in one of the imaging modalities employed in this work.

Combination of imaging modalities increase the robustness of collateral damage assessment. In case, one modality fails to detect collateral damage the other modality could. This can be appreciated by observing Table D.1 in appendix D which shows a case-by-case analysis of 52 operated neurons and the collateral damage detected using various imaging modalities. There were 11 cases out of 52 in which there was no damage detected using fluorescence microscopy, however collateral damage was detected subsequently with post-surgical SHG and MLSBF imaging.

By the currently accepted convention of detecting collateral damage by observing induced autofluorescence there were 33 out of 52 cases which did not show any collateral damage. This puts the success rate of our tool (by the accepted convention) at 63%. However this does not take into consideration the damage to cuticle as well as muscle. By using a more stringent analysis of collateral damage as we are able to do with our system we have 11 out of 52 (about 20%) cases where we donot see any collateral damage at all (no induced autofluorescence, no cuticle damage and no muscle damage).

The techniques described in this chapter for real time observation of the dynamics of the process of Nano-neurosurgery as well as novel tools for accessing collateral damage can in the long run have potential to revolutionize the study of nanosurgery in biological samples using a practical optical workstation convenient to every biologist.